Naval Research Laboratory
Stennis Space Center, MS 39529-5004

NRL/FR/7320--00-9927

Improvement and Validation of the Navy Longshore Current Model

Y. Larry Hsu

Ocean Dynamics and Prediction Branch
Oceanography Division

Theodore R. Mettlach
Marshall D. Earle

Neptune Sciences Incorporated
Slidell, LA 70461

July 13, 2000

REPORT DOCUMENTATION PAGE

Form Approved
OMB No. 0704-0188

1. AGENCY USE ONLY (*Leave Blank*)	2. REPORT DATE	3. REPORT TYPE AND DATES COVERED
	July 13, 2000	

4. TITLE AND SUBTITLE

Improvement and Validation of the Navy Longshore Current Model

5. FUNDING NUMBERS

PE - 0603207N
PN - X2342

6. AUTHOR(S)

Y. Larry Hsu, Theodore R. Mettlach,* and Marshall D. Earle*

7. PERFORMING ORGANIZATION NAME(S) AND ADDRESS(ES)

Naval Research Laboratory
Oceanography Division
Stennis Space Center, MS 39529-5004

8. PERFORMING ORGANIZATION REPORT NUMBER

NRL/FR/7320--00-9927

9. SPONSORING/MONITORING AGENCY NAME(S) AND ADDRESS(ES)

Commander, Space and Naval Warfare Systems Command
PMW 185, 4301 Pacific Highway OT-1
San Diego, CA 92110-3127

10. SPONSORING/MONITORING AGENCY REPORT NUMBER

11. SUPPLEMENTARY NOTES

*Neptune Sciences Incorporated
Slidell, LA 70461

12a. DISTRIBUTION/AVAILABILITY STATEMENT

Approved for public release; distribution is unlimited.

12b. DISTRIBUTION CODE

13. ABSTRACT (*Maximum 200 words*)

The Navy Standard Surf Model, SURF 3.0, is known to have shortcomings in longshore current prediction. Currents are often found to be too weak over most of the surf zone and too high in very shallow water. Both bottom friction and horizontal eddy diffusion formulations in SURF 3.0 are carefully examined and modified. Instead of using a constant friction throughout the surf zone, a new bottom friction function is developed based on water depth and surf zone width. Data acquired during the 1990 Duck Experiment on Low-frequency and Incident-band Longshore and Across-shore Hydrodynamics (DELILAH) and the 1994 DUCK94 experiment are used to derive the optimal empirical constants for the bottom friction and eddy diffusion functions. The implementation of a new bottom-friction function and eddy viscosity coefficient significantly improves the magnitude and location of the maximum current, and greatly reduces the unrealistic high current near the water edge. The new model also produces lower root-mean-square errors. The general accuracy of resulting longshore current estimates is further verified using the 1980 data set from National Sediment Transport Experiment (NSTS), conducted at Leadbetter Beach, Santa Barbara, California. The improved model constitutes significant progress in longshore current prediction and will be used to upgrade the SURF 3.0 model.

14. SUBJECT TERMS

Ocean models
Military oceanography
Surf
Wave

15. NUMBER OF PAGES

46

16. PRICE CODE

17. SECURITY CLASSIFICATION OF REPORT	18. SECURITY CLASSIFICATION OF THIS PAGE	19. SECURITY CLASSIFICATION OF ABSTRACT	20. LIMITATION OF ABSTRACT
UNCLASSIFIED	UNCLASSIFIED	UNCLASSIFIED	UL

NSN 7540-01-280-5500

Standard Form 298 (Rev. 2-89)
Prescribed by ANSI Std 239-18
298-102

CONTENTS

EXECUTIVE SUMMARY

The Navy Standard Surf Model, SURF 3.0, is known to have shortcomings in longshore current prediction. Currents are often found to be too weak over most of the surf zone and too high in very shallow water. Both bottom friction and horizontal eddy diffusion formulations in SURF 3.0 are carefully examined and modified. Instead of using a constant friction throughout the surf zone, a new bottom friction function is developed based on water depth and surf zone width. Data acquired during the 1990 Duck Experiment on Low-frequency and Incident-band Longshore and Across-shore Hydrodynamics (DELILAH) and the 1994 DUCK94 experiment are used to derive the optimal empirical constants for the bottom friction and eddy diffusion functions. The implementation of a new bottom-friction function and eddy viscosity coefficient significantly improves the magnitude and location of the maximum current, and greatly reduces the unrealistic high current near the water edge. The new model also produces lower root-mean-square errors. The general accuracy of resulting longshore current estimates is further verified using the 1980 data set from National Sediment Transport Experiment (NSTS), conducted at Leadbetter Beach, Santa Barbara, California. The improved model constitutes significant progress in longshore current prediction and will be used to upgrade the SURF 3.0 model.

IMPROVEMENT AND VALIDATION OF THE NAVY LONGSHORE CURRENT MODEL

1.0 INTRODUCTION

SURF 3.0 is the latest version of the Navy Standard Surf Model (NSSM). It is a streamlined version of SURF96 that has been modified by Migues et al. (1999) to conform to the programming standards of the Oceanographic and Meteorological Master Library (OAML). SURF3.0 was delivered to the System Integration Department of the U.S. Naval Oceanographic Office (NAVOCEANO) in February 1999. SURF 3.0 has been approved by NAVOCEANO to replace SURF 2.1 as the operational version of the NSSM. This report presents straightforward yet highly effective improvements to the longshore current computations in SURF 3.0.

This report is the latest in a recent series of reports that address various aspects of the NSSM, including validation and alternative initialization methods.

Mettlach and May (1997) examined the accuracy of model-derived modified surf index (MSI). The model used (Mettlach et al., 1996) was a research version of SURF 2.1. It was shown that longshore current is a relatively high contribution to the MSI and that errors in current produce concomitantly high errors in MSI.

May and Mettlach (1997) explored the utility of wave model estimates and depth profile estimates using remote sensing techniques for SURF96 initialization. The accuracy of Navy Wave Model (WAM) nowcasts and forecasts for surf model initialization was examined in detail.

Hsu et al. (1997) conducted a thorough evaluation of SURF96. SURF96 and SURF3.0 produce nearly identical results when certain options in SURF96 conform to the configuration of run parameters set in SURF 3.0. Their model was initialized and evaluated using in situ meteorological, oceanographic, and bathymetry data acquired during two experiments. Four cases from the National Sediment Transport Study (NSTS) conducted at Leadbetter Beach, Santa Barbara, California, during February, 1980—the same four used in this study—were used to examine model accuracy with a planar beach. Seventy-nine cases from the Duck Experiment on Low-frequency and Incident-band Longshore and Across-shore Hydrodynamics (DELILAH), conducted at the U.S. Army Corps of Engineers, Field Research Facility (FRF), Duck, North Carolina, during October 1990 were used to examine model accuracy with a barred beach. These cases are also used in the present report. Two characteristic shortcomings in longshore current estimates were discovered:

- Over most of the surf zone, the calculated longshore current was approximately half of that measured.

- Very near the edge of the water, in water less than 1-m depth, the model often produced a second peak that was larger than the first peak, contrary to measured data. This problem is particularly serious over a planar beach. In the present report, methods to correct both of these shortcomings are given.

Manuscript approved September 30, 1999.

Based on SURF96, Mettlach et al. (1999) estimated surf zone width. More than 600 surf zone width determinations from 10-min averaged video records were optimally correlated to the most offshore location where the surf model estimated 10 percent wave breaking to occur. This simple method produced mean surf zone width errors of –2 m, with a standard deviation of 30 m. Video-determined widths ranged from 5 to 408 m. In the present study, it is shown that model-derived surf zone width can be effectively used to improve longshore current estimates in SURF3.0.

Lundberg et al. (1997, 1999) have developed a semi-empirical longshore current model that does not need bottom depth as input. In their model, the shape of the longshore current profile in the cross-shore direction is assumed. The current is near zero at a distance of two surf zone widths from the beach, steadily increases to a maximum at a distance of one-half surf zone width, and then steeply decreases to zero at the beach. Model skill is derived largely from the fact that longshore current profiles generally match this bell shape over both planar beaches and barred beaches.

This report shows that longshore current estimates from SURF 3.0 can be improved considerably by replacing a constant bottom friction coefficient with a variable bottom friction function based on surf zone width. The empirical constants for bottom friction and horizontal eddy viscosity are derived based on field data. The improved model is proven to be robust.

2.0 DESCRIPTION OF SURF 3.0

This section describes wave transformation, wave setup, and longshore current formulations used in SURF 3.0. The main assumption governing these equations is that there is along-shore uniformity in depth. Numerical methods for computing the solutions of the differential equations representing wave transformation and longshore current are described in detail. Empirical constants used in the model are given.

Wave breaking and transformation is based on the concept that organized wave motion at breaking is converted to a turbulent roller riding over the underlying wave. The production and advection of wave energy balances the dissipation of wave energy. The equations for wave transformation using roller theory are taken from Lippmann et al. (1996), which is based on the parametric wave transformation model of Thornton and Guza (1983).

The longshore current model is based on the radiation stress theory of Longuet-Higgins (1970a, 1970b), with an added term for wind stress given in Earle (1991). The numerical solution for longshore current uses Gaussian elimination of a tri-diagonal matrix, which is given in Kraus and Larson (1991).

2.1 Wave Transformation

The energy flux equation balances the wave and roller fluxes of energy density to energy dissipation ε,

$$\frac{d\left(E_w c_g \cos\theta\right)}{dx} + \frac{d\left(E_r c \cos\theta\right)}{dx} = -\varepsilon. \tag{1}$$

The energy of incoming waves E_w travels at the wave group velocity c_g, and rollers, which are associated with depth-limited breaking, are assumed to travel at the phase velocity of the wave c. Using linear wave theory, the wave energy per unit area of sea surface in a distribution of waves with root-mean-square wave height H_{rms} is given as

$$E_w = \frac{1}{8}\rho g H_{rms}^2, \tag{2}$$

with g being the acceleration due to gravity (9.81 m/s^2) and ρ the density of seawater (1030 kg/m^3). Linear wave theory also yields the following relationships among wave energy speed c_g, angular frequency ω, radian wave number k, wave phase speed c, depth h, wave frequency f, and wavelength L:

$$c_g = \frac{d\omega}{dk} = c\left(\frac{1}{2} + \frac{kh}{\sinh 2kh}\right); \tag{3}$$

$$c = \frac{\omega}{k} = fL; \tag{4}$$

$$\omega^2 = gk \tanh kh. \tag{5}$$

Using the assumption that depth contours in the nearshore are locally straight and parallel to the beach, then Snell's law can be used to compute wave direction θ if the offshore wave angle θ_o and its frequency and depth are known.

$$\frac{\sin\theta}{c} = \frac{\sin\theta_0}{c_0}. \tag{6}$$

The surf model is initialized with the measured or estimated wave height, period, and direction at an offshore point. These wave parameters are best derived from a complete directional wave spectrum $S(f,\theta)$. The root-mean-square wave height H_{rms} is computed from the zero moment of wave variance,

$$H_{rms} = \frac{H_{mo}}{\sqrt{2}} = \left(8 \int_{-\pi/2}^{\pi/2} \int_{0}^{\infty} S(f,\theta) df d\theta\right)^{\frac{1}{2}}. \tag{7}$$

The peak wave frequency in the spectrum is that frequency band with a maximum in energy,

$$f_p = f\left(\max\left[\int_{-\pi/2}^{\pi/2} S(f,\theta) d\theta\right]\right). \tag{8}$$

It is used for model initialization and is assumed conserved throughout the surf zone.

The wave angle used for model initialization θ_o is computed from the total energy of the input wave spectrum and the total energy of the along shore component of cross shore radiation stress $S_{xy}(f,\theta)$, i.e.,

$$\theta_0 = \frac{1}{2}\sin^{-1}\left[\frac{2\int_{-\pi/2}^{\pi/2}\int_{0}^{\infty} S_{xy}(f,\theta) df d\theta}{\int_{-\pi/2}^{\pi/2}\int_{0}^{\infty} S(f,\theta) df d\theta \left(\frac{1}{2}\left[1 + \frac{2k(f_p,h)h}{\sinh 2k(f_p,h)h}\right]\right)}\right]. \tag{9}$$

$$S_{xy}(f,\theta) = S(f,\theta)\left[\frac{1}{2} + \frac{k(f,h)h}{\sinh 2k(f,h)h}\right]\cos\theta\sin\theta. \tag{10}$$

Because of wave refraction, most wave angles will be within 45 deg of shore normal. Because of the relatively small wave angles in the surf zone, errors in wave angle produce relatively greater errors in longshore current than in wave height because wave height is proportional to the cosine of the wave angle while the longshore current is proportional to its sine. If, for example, the true wave angle is 20 deg but the wave angle used in the model is 10 deg, then there will be a 4.7 percent error in wave height, but a –49.2 percent error in longshore current. It is stressed that changes in the definition of wave angle may have significant effects on longshore current estimates.

Surface roller energy density is given as

$$E_r = \frac{1}{2}\rho_r c^2 \frac{A}{L}. \tag{11}$$

This equation is derived from the kinetic energy density of the roller volume, i.e., from $mv^2/2$, where v is assumed to be the speed of travel of the roller, which is the phase speed of the underlying wave. The kinetic energy density is found relative to a unit wavelength and the surface area A of the roller covering the face of the underlying, breaking wave,

$$A = \frac{H_b^3}{4h\tan\sigma}. \tag{12}$$

This area is approximated from the root-mean-square wave height at the time of wave breaking H_b, local bottom depth h, and the angle of the wave-roller stress vector σ, which gives the slope of the wave front. The density of aerated water comprising the roller ρ_r is less than that of the water in the underlying wave below the roller, although the density of seawater ρ is used as a simplification. H_b is actually H_{rms} in model calculations of A.

Energy dissipation is assumed to occur exclusively at the shear surface interface between the roller and the organized, underlying wave. Bottom friction is neglected. The turbulent kinetic energy (TKE) per unit area produced at the wave-roller interface is given as

$$\tau_s = \rho g A \sin\sigma. \tag{13}$$

Thus, energy loss per horizontal surface area and per unit time ε (with units W/m^2) is given as

$$\varepsilon = \frac{\tau_s c}{L} = \frac{1}{4}\rho g f_p \frac{H_b^3}{h}\cos\sigma. \tag{14}$$

Energy dissipation is calculated by accounting for changes in breaker wave height $H_b (= H_{rms})$ throughout the surf zone, which are functionally related to the probability density that a wave of a given height is either breaking or broken. The probability density $p_b(H)$ that a wave of given height H is either breaking or broken,

$$p_b(H) = W(H)p(H), \tag{15}$$

is found from a Rayleigh probability density distribution $p(H)$, i.e.,

$$p(H) = \frac{2H}{H_{rms}^2} e^{-\left(\frac{H}{H_{rms}}\right)^2}, \tag{16}$$

multiplied by a factor $W(H)$, which is an empirically derived weighting function. In SURF 3.0 the following weighting function is used,

$$W(H) = \left(\frac{H_{rms}}{\gamma h}\right)^4 \left(1 - e^{-\left(\frac{H}{\gamma h}\right)^2}\right) \leq 1, \tag{17}$$

where $\gamma = 0.42$ represents a constant ratio between H_{rms} and h. This weighting function is taken from Thornton and Guza (1983), who derived it from a limited set of wave distributions that contained breaking and nonbreaking waves.

In the model, the cubed breaker wave height is calculated numerically using a trapezoidal integration from 0 to $5H_{rms}$,

$$H_b^3 = \int_0^\infty H^3 p_b(H) dH \cong \sum_{H=0}^{5H_{rms}} H^3 p_b(H) \Delta H. \tag{18}$$

The energy flux balance equation is solved using a forward-stepping numerical function from offshore to the edge of the water in increments of Δx,

$$(E_w c_g \cos\theta)_2 + (E_r c \cos\theta)_2 = \Delta x \varepsilon + (E_w c_g \cos\theta)_1 + (E_r c \cos\theta)_1. \tag{19}$$

Subscripts 1 and 2 indicate points in cross-shore direction, with 1 being farther offshore than 2. The equation is balanced by finding $H_{rms,2}$ with an iterative solution.

2.2 Wave Setup

Setup of the mean water level η is given by

$$\frac{dS_{xx,w}}{dx} + \frac{dS_{xx,r}}{dx} + \rho g h \frac{d\eta}{dx} = 0. \tag{20}$$

The first term is the gradient in radiation stress due to wave motion, and the second term is that due to roller motion. The third term is the pressure gradient from setup. The wave contribution to radiation stress is

$$S_{xx,w} = \left(\frac{c_g}{c}\left(1 + \cos^2\theta\right) - \frac{1}{2}\right) E_w. \tag{21}$$

The roller momentum flux is

$$S_{xx,r} = 2E_r \cos^2 \theta. \tag{22}$$

In SURF 3.0, the setup is added to the mean water level to compute wave height. A simple forward finite-difference numerical function is used to compute setup.

2.3 Longshore Current

The longshore current model used in SURF 3.0 balances the longshore (y-directed) momentum flux from waves in the surf zone τ_H, the horizontal exchange of momentum due to turbulent mixing, the dissipation of momentum due to bottom friction τ_B, and the generation of momentum from the wind τ_U,

$$\tau_H + \rho \frac{d}{dx}\left(h\nu_t \frac{dV}{dx}\right) - \tau_B + \tau_U = 0. \tag{23}$$

Wave input for the momentum balance equation is given by

$$\tau_H = \varepsilon \frac{\sin\theta}{c}. \tag{24}$$

In the second term of the momentum balance equation, lateral or horizontal eddy viscosity is represented by (Battjes, 1975)

$$\nu_t = Mh\left(\frac{\varepsilon}{\rho}\right)^{1/3}, \tag{25}$$

such that M is an empirical constant, and is set to 2 in SURF 3.0.

The bottom shear stress term is modeled simply as

$$\tau_B = c_f \rho u V. \tag{26}$$

The bottom drag coefficient c_f = 0.007 is constant throughout the surf zone. It is shown later that using a variable bottom friction coefficient function improves model estimates compared to field data. This is intuitively reasonable in that there is often preferential sorting of sediment material by grain size in the surf zone, yielding areas of relatively coarse sand in the swash zone and progressively finer sand with greater depth and distance offshore.

The variable u is the magnitude of the near-bottom horizontal wave orbital velocity,

$$u = \frac{\sqrt{\pi} f_p H_{rms}}{\sinh kh}. \tag{27}$$

Finally, the wind stress from a wind of speed U and direction θ_U is

$$\tau_U = U^2 \sin\theta_U \rho_a c_d, \tag{28}$$

$\rho_a = 1.2$ g/m^3, and

$$c_d = \begin{matrix} 1.2875\times10^{-3} & U \le 7.5\,\text{m/s} \\ (0.8+0.065U)10^{-3} & U > 7.5\,\text{m/s} \end{matrix}. \tag{29}$$

The longshore current is computed numerically using three passes across the cross-shore grid representing the surf zone. In the first pass, energy dissipation and wave height are computed. Three intermediate variables A_i, B_i, and Ci are also computed during this pass, which proceeds from offshore, where i =1, to near the water's edge, where $i = N$. These intermediate variables are given as:

$$A_i = M\rho h_i^2 \left(\frac{\varepsilon_i}{\rho}\right)^{1/3} \tag{30}$$

$$B_i = \frac{c_f \rho f_p \sqrt{\pi} H_{rms,i}}{\sinh k_i h_i} \tag{31}$$

$$C_i = \frac{-\varepsilon_i \sin\theta_i}{c_i} - U^2 \sin\theta_U \rho_a c_d. \tag{32}$$

In the second pass, the two intermediate variables E_i and F_i are computed. This pass proceeds from near the beach, where $i = N-1$ to offshore, where $i = 2$:

$$E_i = \frac{A_{i-1}}{B_i \Delta x^2 + A_{i-1} + A_i\left(1 - E_{i+1}\right)}, \tag{33}$$

$$F_i = \frac{A_i F_{i+1} - C_i \Delta x^2}{B_i \Delta x^2 + A_{i-1} + A_i\left(1 - E_{i+1}\right)}. \tag{34}$$

At the beach,

$$E_N = 0 \tag{35}$$

and

$$F_N = \frac{\varepsilon_N}{B_N} \frac{\sin\theta_o}{c_o}. \tag{36}$$

The third pass yields the model's estimate of longshore current V_i from $i = 2$ to $i = N$. This pass proceeds from offshore to near the beach,

$$V_i = E_i V_{i-1} + F_i . \tag{37}$$

This pass begins with the steady-state wind-generated current V_1,

$$V_1 = \sqrt{\frac{\rho_a}{\rho}} \frac{c_d}{c_f} U \sin\theta_U . \tag{38}$$

3.0 MODEL EVALUATION OF SURF 3.0

This section summarizes an evaluation of the accuracy of SURF 3.0 in estimating H and V. This is done using wave height and longshore current measurements acquired during DELILAH and DUCK94. The model is initialized with depth, tide, ζ, and offshore wave and wind measurements from these experiments.

Because of the demands that are placed on the operational performance of the NSSM, it is imperative that it be tested under a wide range of wind and wave conditions. The combined DELILAH-DUCK94 data set is used for such testing. Of the cases selected from these two field experiments, the wind speed ranged from 1 to 12 m/s, and the offshore significant wave height ranged from 0.4 to 4.0 m. Figures 1 and 2 give time series of wind speed, wave height, wave direction, and peak wave period of the cases used in this study.

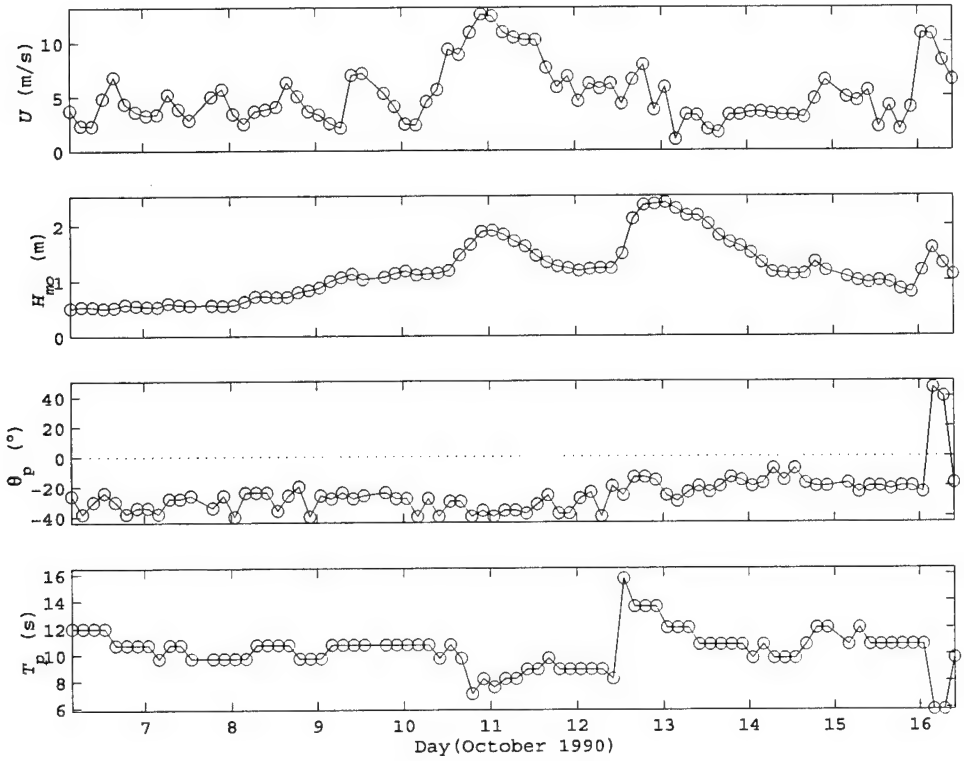

Fig. 1 — Wind and wave measurements for 79 DELILAH cases—wind speed, significant offshore wave height, peak wave direction, and peak wave period

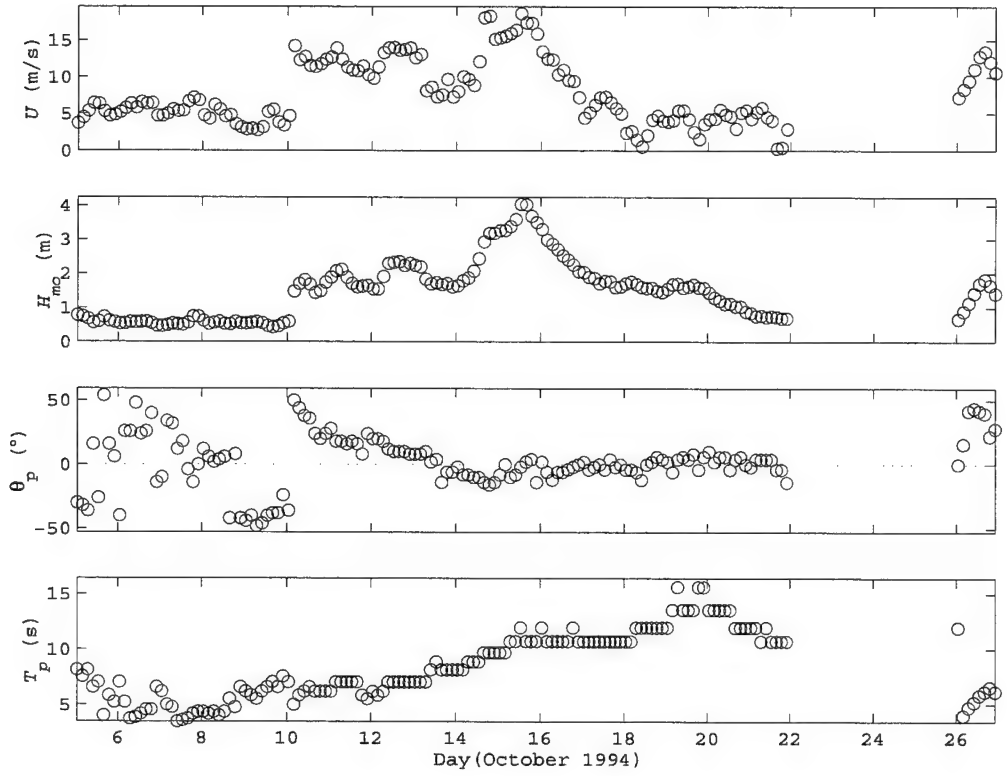

Fig. 2 — Wind and wave measurements for 144 DUCK94 cases—wind speed, significant offshore wave height, peak wave direction, and peak wave period

The beach at the FRF is representative of many beaches of interest to the Navy. The nearshore gradient number at Duck, depending on the along-shore location, ranges from approximately 85 to 105, with a mean of 94. The gradient number is a single dimensionless number $\Delta x/30$, where Δx is the distance from the beach in feet to a depth of 30 ft. Using an unclassified listing based on the *Defense Planning Guide* (DPG), which contains distance to depth of 30 ft for 248 potential landing sites, Mettlach et al. (1999) have shown that the median beach gradient number in the DPG data set is 92, in which the values range from 8 to 2411. Approximately 70% of the DPG gradient numbers are between 25 and 200. This median value is very close to that at Duck.

The conditions during the two experiments are markedly different in one particular way—the averaged peak wave direction θ_p during DELILAH was from –24.9 deg (positive counterclockwise from shore normal, seaward (070 deg north), while during DUCK94, the averaged peak wave direction was +2.6 deg. The peak wave direction is defined as that direction in which there is a maximum in wave energy. During DELILAH, the long pier south of the surf zone observation area may have affected longshore current development from these waves arriving from the southeast. During DUCK94, the frequent occurrence of waves directly onshore, of course, produces very small longshore currents. Also, very high winds during DUCK94 could have set up non-wave-driven strong coastal currents in ways that are not considered by the model physics.

3.1 Wave Height

Figure 3 is a scatter plot of the root-mean-square wave heights acquired during DELILAH and DUCK94 vs the corresponding model estimates. The sensor description and arrangement is easily accessible from the

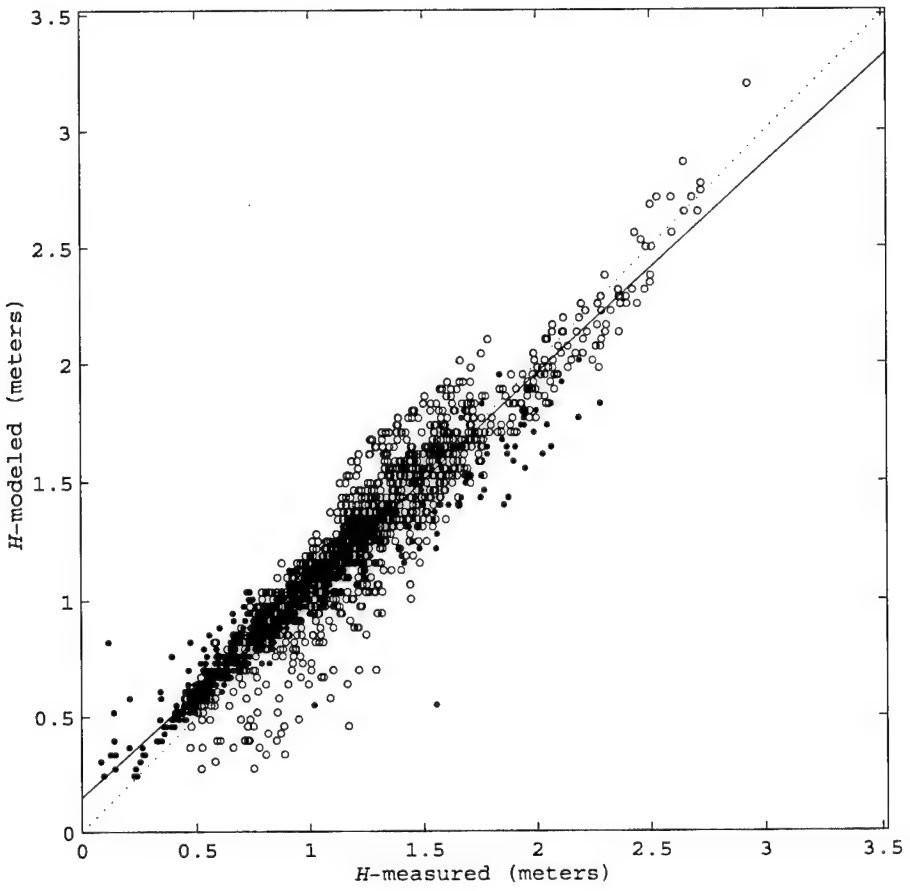

Fig. 3 — Scatter diagram of measured root-mean-square wave heights vs estimates of wave height. Dots denote DELILAH measurements; circles denote DUCK94 measurements. N = 1796 observations. Skill statistics based on model minus measured differences of set from combined data sets are: linear correlation coefficient $R = 0.945$; minimum error $\varepsilon_{min} = -1.01$ m; mean error $\varepsilon_{mean} = 0.04$ m; maximum error $\varepsilon_{max} = 0.71$ m; standard deviation of the errors σ = 0.15 m; mean fractional error $\varepsilon_{100} = 6.2\%$; mean of the absolute values of the fractional error $\varepsilon_{100abs} = 12.5$ %. The solid line is a linear regression curve with slope $m = 0.90$, and y-intercept $b = 0.15$ m.

Corps of Engineers Web site, therefore is not repeated here. The skill of the model is quite high, with a mean percent error of +6.2 percent, which is close to the minimum error found by Lippmann et al. (1996) using just nine cases. The model was run with the standard model parameters given in Section 3.0, i.e., $\gamma = 0.42$ and $\sigma = 5°$. For this validation, the *Self Start* option of the model (see Hsu et al., 1997) was used. The *Self Start* option suppresses wave energy dissipation until a threshold of 5 percent wave breaking occurs. It is noted that the slope of the best-fitted linear regression curve through the measurement-model pairs has a y-intercept of +0.15 m/s and a slope m of 0.90, which suggests that true wave heights above 1.5 m are underestimated by the model.

An additional series of 15 sets of surf model runs using the DELILAH and DUCK94 data sets were made to examine the sensitivity of the model to its two wave energy dissipation parameters—γ and σ [Eq. (17) and Eqs. (12)-(14)], respectively). This examination is analogous to that made by Lippmann et al. (1996), who calculated the percentage of error between modeled and measured wave height for individual surf zone measurement cases. It the present examination the percentage of error and several other skill statistics are calculated for combinations of γ and σ for γ ranging from 0.3 to 0.5 and σ ranging from 2° to 6°.

The results are given in Table 1, which shows that the optimal combination of γ and σ is $\gamma = 0.40$ and $\sigma = 6°$, which is very close to the standard values used in the model. Note that unlike the set of runs represented in Fig. 3, the additional sensitivity study has been done without the *Self Start* option, allowing a uniform number of validating measurements for each set of runs ($N = 2660$). The higher skill for $\gamma = 0.42$ and $\sigma = 5°$ in Table 1 (than given in the caption of Fig. 3) is due to the greater number of wave measurements farther offshore being incorporated into the validation (than the fewer number of measurements (N =1796) from the runs with the *Self Start* option).

3.2 Longshore Current

Figure 4 is a similar plot of longshore current measurements from DELILAH and DUCK94 vs the corresponding model estimate. The skill of the model in estimating V is much less than that of the model in estimating H_{rms}. The most striking feature is the low value of slope ($m = 0.48$), indicating underprediction of currents. The statistics listed under the figure caption are discussed in Section 5.2.

Table 1 — Skill Statistics from 15 Sets of Surf Model Run Using Values of γ and σ (°) Noted.

γ	σ	N	R	ε_{min}	ε_{mean}	ε_{max}	σ	ε_{100}	ε_{100abs}	m	b
.30	2	2660	0.942	-1.038	-0.112	0.614	0.165	-6.832	13.36	0.768	0.131
.30	4	2660	0.946	-1.038	-0.130	0.584	0.170	-8.212	14.35	0.723	0.160
.30	6	2660	0.946	-1.038	-0.136	0.553	0.175	-8.703	14.87	0.707	0.170
.36	5	2660	0.960	-1.007	-0.045	0.645	0.137	-0.663	10.46	0.821	0.143
.37	5	2660	0.961	-1.007	-0.042	0.645	0.137	-0.381	10.44	0.822	0.145
.38	5	2660	0.961	-1.007	-0.039	0.675	0.136	-0.094	10.48	0.822	0.147
.39	5	2660	0.961	-1.007	-0.037	0.675	0.136	0.186	10.53	0.823	0.148
.40	2	2660	0.951	-1.007	0.018	0.706	0.141	4.692	11.56	0.908	0.113
.40	5	2660	0.961	-1.007	-0.034	0.675	0.136	0.437	10.59	0.824	0.150
.40	6	2660	0.962	-1.007	0.006	0.675	0.126	3.753	10.27	0.882	0.130
.41	5	2660	0.961	-1.007	-0.032	0.706	0.136	0.714	10.70	0.824	0.152
.42	5	2660	0.960	-1.007	-0.030	0.706	0.136	0.958	10.81	0.825	0.154
.50	2	2660	0.942	-1.007	0.117	0.797	0.166	13.523	16.56	1.017	0.099
.50	4	2660	0.951	-1.007	0.115	0.767	0.152	13.257	16.08	1.014	0.100
.50	6	2660	0.953	-1.007	0.114	0.767	0.148	13.120	15.86	1.014	0.099

γ = coefficient used with Thornton and Guza wave dissipation model
σ = angle of the wave-roller stress vector (degrees)
N = number if model-measurements pairs
R = linear correlation coefficient between model estimates and measurements
ε_{min} = minimum error (m)
ε_{mean} = simple mean of the individual errors (model - measurement) (m)
ε_{max} = maximum error (m)
σ = standard deviation of the error (± m)
ε_{100} = 100 × mean fractional error ([model-meas.])/meas.; meas. ≠ 0)
ε_{100abs} = 100 × mean absolute value of fractional error ([model-meas.]/meas.; meas. ≠ 0)
m = slope of regression line through model-measurement pairs
b = y-intercept. Offset of regression line through model-measurement pairs (m)

N is number of measurement-model estimate pairs from the set of surf model runs. Linear correlation coefficient is R. Minimum error is ε_{min} (m). Mean error is ε_{mean} (m). Maximum error is ε_{max} (m). Standard deviation of error is σ (m), which should not be confused with the angle σ. Mean fractional error in percent is ε_{100}. Mean of the absolute values of the fractional error in percent is ε_{100abs} (%) Slope of regression curve through model-measurement pairs is m. Y-intercept of regression curve is b (m).

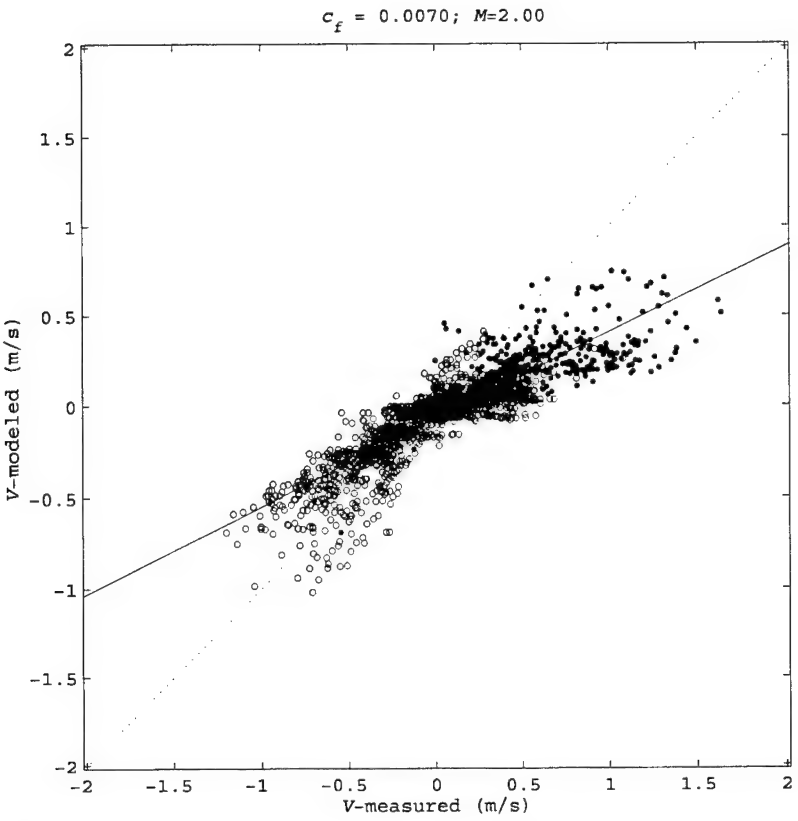

Fig. 4 — Scatter diagram of measured longshore currents vs corresponding model estimates of current. Dots denote DELILAH measurements; circles denote DUCK94 measurements. N = 1930 observations. Skill statistics based on model minus measured differences of set from combined data sets are: linear correlation coefficient R = 0.87; minimum error ε_{min} = –1.15 m/s; mean error ε_{mean} = –0.10 m/s; maximum error ε_{max} = 0.57 m/s; standard deviation of the errors σ = 0.27 m/s; mean fractional error ε_{100} = –49.9 %; mean of the absolute values of the fractional error ε_{100abs} = 97.5 %. The solid line is a linear regression curve with slope m = 0.48 and y-intercept b = –0.07 m/s.

Accurate estimates of the maximum current in the surf zone V_{max} are important with regard to modified surf index (MSI) computations. MSI, defined in the *Joint Surf Manual* (Commander, Naval Surface Force, Pacific and Commander, Naval Surface Force, Atlantic, 1987) is the sum of weighted, nondimensional values of surf parameters. These include wave height, wave period, wave direction relative to the beach, V_{max}, breaker type and wind speed. Each foot of wave height contributes 1 MSI unit to the total. Each knot of longshore current contributes 3 MSI units. In Fig. 5, measured V_{max} from the DELILAH and DUCK94 cases are plotted against the corresponding SURF 3.0-modeled V_{max}. The statistics of Fig. 5 are similar to Fig. 4. It should be noted that the slightly improved values are due to the fact that some computed V_{max} are located at the end of the beach, far from the measured peak near the middle of surf zone. Those values probably should not be considered as valid values in computing the statistics.

4.0 PARAMETERIZATIONS IN LONGSHORE CURRENT MODEL

Physical processes in the surf zone are especially complex and require some degree of parameterization for efficient modeling. The set of equations given in Section 2.0 relies on several empirical parameters and parameterizations for closure, two of which are discussed in this section: c_f and ν_t.

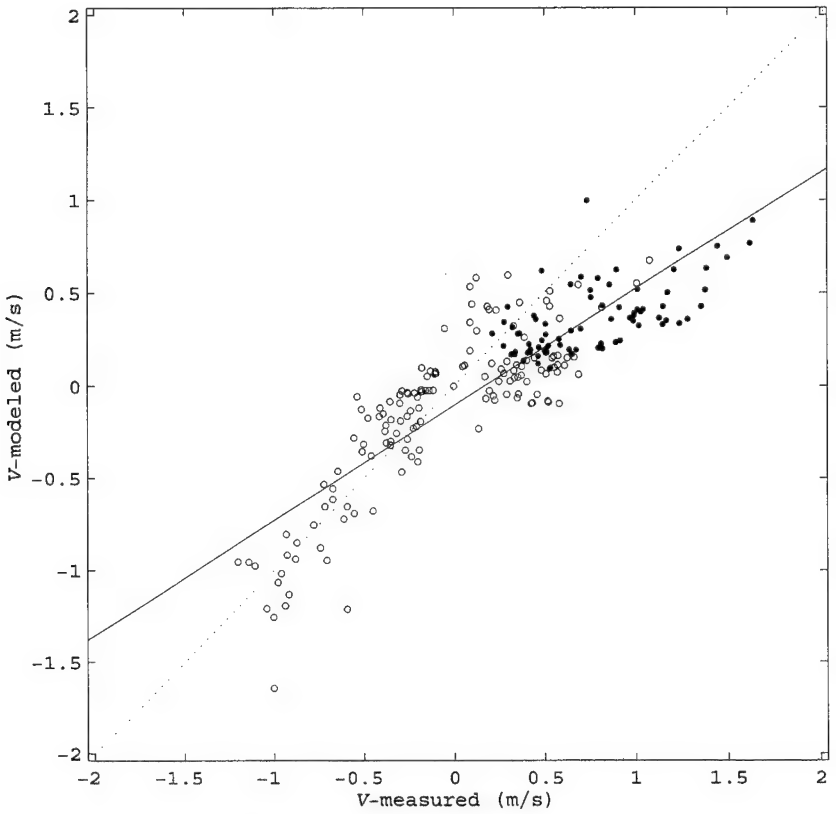

Fig. 5 — Scatter diagram of maximum measured longshore currents vs the corresponding maximum model estimates of current. Dots denote DELILAH measurements; circles denote DUCK94 measurements. N = 223 observations. Skill statistics based on model minus measured differences of set from combined data sets are: linear correlation coefficient R = 0.86; minimum error ε_{min} = –0.93 m/s; mean error ε_{mean} = –0.19 m/s; maximum error ε_{max} = 0.48 m/s; standard deviation of the errors σ = 0.32 m/s; mean fractional error ε_{100} = –40.1 %; mean of the absolute values of the fractional error ε_{100abs} = 74.2 %. The solid line is a linear regression curve with slope m = 0.63 and y-intercept b = –0.1 m/s

4.1 Bottom Friction Coefficient c_f

The value of the bottom friction coefficient c_f is the main fitting parameter in longshore current modeling. The value used in SURF 3.0 is the same value used in previous versions of the navy model, i.e., c_f = 0.007, constant throughout the surf zone (Earle, 1991).

Thornton and Guza (1986) in citing Shemdin et al. (1978) state that reported values of c_f range between 0.005 to 0.3. Thornton and Guza, under the assumption of a constant c_f in the surf zone, determined optimal values of c_f from four field cases by solving through trial and error the least-square error between calculated and measured longshore current values shoreward of the mean breaker line. For a linear bottom stress formulation of longshore current, similar to that used in SURF96, their optimal values ranged from 0.005 to 0.009. For the same four cases, using a similar linear bottom stress model, Kraus and Larson (1991) found optimal values ranging from 0.004 to 0.006. Reniers and Battjes (1997) in a laboratory study of longshore currents over a barred beach found that c_f = 0.007, constant was an optimal value for a linear model incorporating rollers in the energy dissipation calculations.

Smith et al. (1993) examined three candidate forms of c_f. The first was to assume that c_f is a constant value. The second was to use the wave friction coefficient of Jonsson (1966), which was used by Thornton (1970) and is given by

$$\frac{1}{4\sqrt{c_f}} + \log\frac{1}{4\sqrt{c_f}} = -0.08 + \log\frac{\xi}{r}, \tag{39}$$

in which ξ is the maximum water particle excursion amplitude of fluid motion at the bottom as predicted by linear wave theory, i.e.,

$$\xi = \frac{H}{2}\frac{1}{\sinh kh}; \tag{40}$$

and r is a roughness parameter, being the measure of ripple height. Third, the Manning friction coefficient

$$c_f = g\frac{n^2}{d^{1/3}} \tag{41}$$

was used. In this formulation, n is an empirically determined coefficient, called the Manning resistance coefficient, and d is the hydraulic radius of wide open-channel flow. Of the three formulations, the Manning friction coefficient was found to produce the least error in longshore current. Smith et al. (1993) do not clearly define d, but do show in a plot from DELILAH (14 October 1990 0100 EST) the Manning friction coefficient ranging from $c_f \cong 0.0022$ far offshore, where $h > 10$ m to $c_f > 0.06$ near the edge of the water. The lower value is less than those mentioned in Thornton and Guza (1986) or Kraus and Larson (1991).

Sancho (1999), who examined unsteady nearshore currents on longshore varying topographies with DELILAH measurements, used an approximation of Eq. (39) based on Swart (1974). For the 0400 UTC 10 October 1990 case, estimates for c_f ranged from 0.006 offshore to 0.017 at the shoreline.

During the SUPERDUCK experiment conducted at the FRF in October 1986, Whitford and Thornton (1986) derived quantitative estimates of various terms in the momentum equation governing the mean alongshore flow in the surf zone. An instrumented sled acquired mean current and bottom shear stress measurements at various locations across the surf zone. Coefficients of c_f were estimated to range from 0.004 seaward of the bar, to 0.003 at the crest of the bar, to 0.001 over the trough shoreward of the bar. It is shown that the shoreward decrease in c_f is statistically significant and suggested to have been due to decreasing wave action shoreward.

More recently, Garcez Faria et al. (1998) have produced another formulation for c_f from field data, one that is dependent on depth and k_a, an apparent bed roughness length scale:

$$c_f = 0.011\left(\frac{k_a}{h}\right)^{1/2.75}. \tag{42}$$

This formula is based on field measurements of c_f acquired at Duck during three strong current days during DUCK94. c_f ranged by more than an order of magnitude (0.0006 – 0.0120). As shown in Fig. 6, c_f tends to

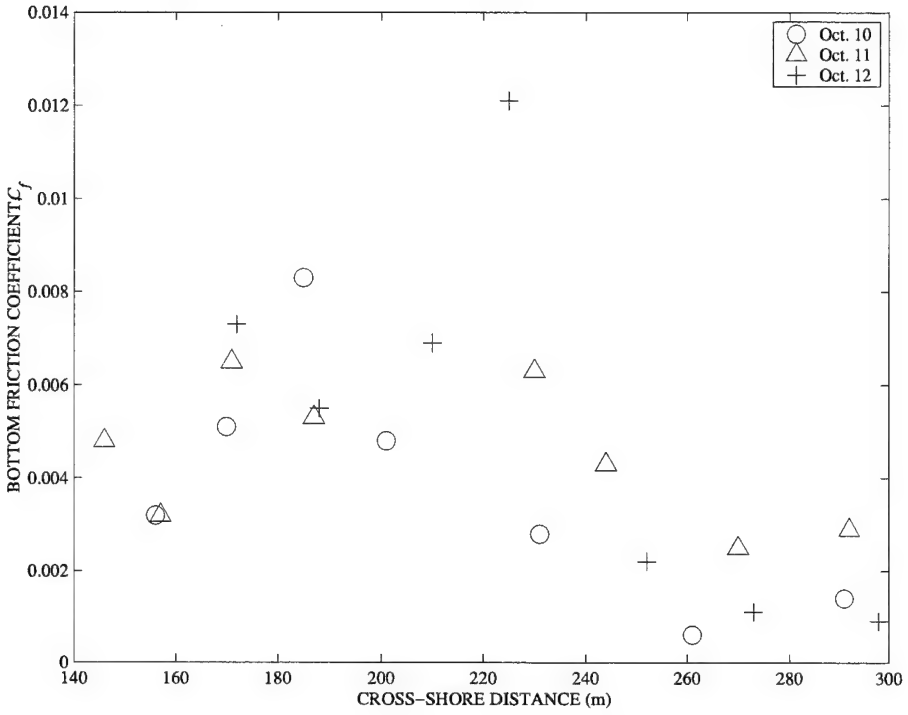

Fig. 6 — Measurements of c_f acquired by Garcez Faria et al. (1998) at Duck, North Carolina, during DUCK94. (Cross-shore distance is relative to a fixed location at the Field Research Facility (FRF) at Duck, North Carolina.) Depending on tide, the edge of the water is located at 100-120 m.

increase shoreward due to increasing bottom form irregularities shoreward. There was a noticeable transition from a smooth, near-planar bottom form seaward of the bar, to rough mega ripples over the bar, to less rough wave ripples very near the beach. Unfortunately, Eq. (42) cannot be easily used in numerical models because apparent bed roughness cannot be known without detailed velocity profile measurement.

In view of the wide range of formulations for bottom friction and its great importance in longshore current estimates, which is shown later in this report, a practical formulation for c_f is developed. This formulation greatly reduces spuriously high estimates of V in very shallow water and increases V to values much closer to measurements over the great majority of the surf zone.

4.2 Parameterization of Lateral Eddy Viscosity ν_t

The lateral eddy viscosity ν_t is also an important empirical parameter in longshore current models. Thornton and Guza (1986) used

$$\nu_t = N \mid x \mid \sqrt{gh} \tag{43}$$

where N is an adjustable coefficient ($0 < N < 0.016$) and x is distance offshore. Implicit in this formula is that mixing length, and, thus, mixing increases with distance offshore.

Kraus and Larson (1991) and Smith et al. (1993) also use a formula for eddy viscosity that contains an empirical coefficient Λ. The formula assumes that mixing is primarily a function of orbital wave motions, i.e.,

$$\nu_t = \Lambda u_m H; \tag{44}$$

u_m is magnitude of the horizontal water particle velocity.

Earle (1991), who considered three formulas for eddy viscosity, accomplished the inclusion of lateral mixing in NSSM. The formula given by Eq. (25) was selected because the dependence on horizontal eddy viscosity on the wave breaking dissipation rate is intuitively satisfying. The M value used in SURF 3.0 is 2.

Changes in M yield changes in the shape of the V profile and in the magnitude of the highest estimated value of V. In view of the importance of M in producing accurate estimates of ν, this value is re-examined in this report using a greater number of field cases than used in previous studies.

5.0 LONGSHORE CURRENT MODEL IMPROVEMENTS

A characteristic problem in SURF 3.0 is that currents are generally too weak in the main portion of the surf zone but often unreasonably high in very shallow water. This first deficiency is demonstrated using simple statistical analysis of model errors. By showing that model estimates of wave height are largely correct, it is inferred that energy dissipation processes are treated adequately. Therefore, the wave momentum input is correct, and the deficiency is from the longshore current model itself.

Careful troubleshooting of the actual model code, tests of the algorithms on which the software is based, e.g., numerical solutions of differential equations, and review of the theory, revealed no apparent underlying causes for these model deficiencies. Simply decreasing c_f to another constant value does not produce accurate results because doing so does not effectively change the shape of the longshore current profile. That is, lowering c_f will increase currents over most of the surf zone but at the expense of exacerbating the unreasonably high currents in very shallow water. Recent measurements of c_f imply that a variable bottom friction function instead of fixed constant may be necessary. But no existing formulation can produce consistently good results.

A first step toward an improved algorithm is to recognize that the maximum longshore current is often near the middle of the surf zone. This has often been an approximation in earlier models theoretically applicable to planar beaches (e.g., Longuet-Higgins, 1970a, 1970b). Lundberg et al. (1997) used the fact that often over a barred beach the maximum longshore current exists near mid surf zone. This phenomenon is especially evident in the records from DELILAH, in which the current maximum is often over the trough, where gradient of radiation stresses are at a minimum.

Figure 7 summarizes the maximum longshore current locations normalized by computed surf zone width for all DELILAH and DUCK94 cases. Cases in which the edge of the surf zone is estimated to extend seaward of the model starting depth are not used. The mean ratios from DELILAH and DUCK94 of the location where there is a maximum current in the surf zone $x(\max|V|)$ to the width of the surf zone X_b are approximately 0.4 from both data sets. The figure shows the mean value of the ratio (solid line) and the one standard deviation from the mean (dotted lines). There is nearly the same scatter from both data sets.

The use of the model to estimate surf zone width is based on the recent work of Mettlach et al. (1999), who showed that SURF96 accurately estimates surf zone width. They analyzed 658 video images to obtain the location of incipient wave breaking and then compared those locations to model output to derive the optimal, percent-breaking threshold from the Navy model. It is important to note that this video work was done using SURF96 with the same options and free parameters for wave transformation and energy dissipation as in SURF 3.0: rollers; $W(H)$ in the form of Eq.(17); $\gamma = 0.42$; $\sigma = 5°$. Surf zone width is estimated to

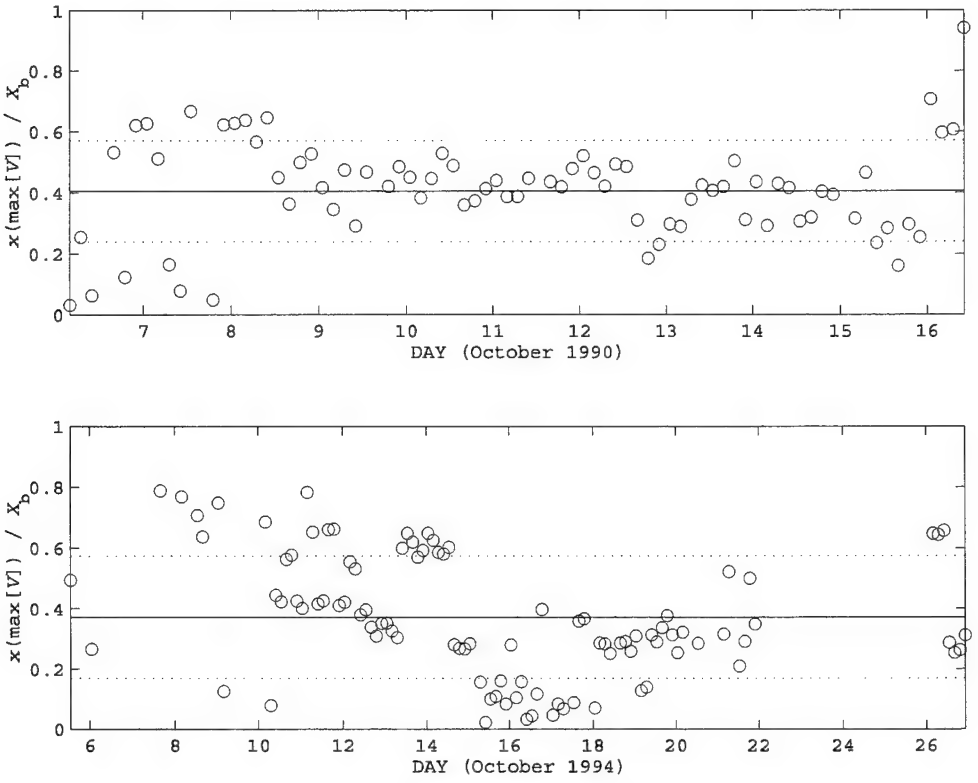

Fig. 7 — Time series of relative location of maximum longshore currents within the estimated surf zone. Solid horizontal line denotes mean; dotted lines denote mean plus and minus one standard deviation from the mean.

start at offshore locations where 10 percent of waves are estimated to be breaking or broken. From the video determinations of surf zone width, using a 10 percent threshold, the model produced width estimates with an expected error of –2 m and one standard deviation of 30 m over a range 5 to 408 m.

With the observation that a current maximum exists near mid surf zone, the next step is to select a functional form for c_f that will tend to produce a maximum in this region. Keeping c_f a constant, relatively low value seaward of the mid surf zone, should increase the maximum current estimate. The next logical parameterization of c_f is to steadily increase it from mid surf zone to the edge of the water. This is accomplished by making c_f inversely related to depth h, which has been done by Smith et al. (1993) with the Manning friction coefficient, Eq. (41), and by Garcez Faria et al. (1998). Increasing friction toward the water edge effectively reduces currents in very shallow water.

5.1 Development of a Variable Bottom Friction Coefficient Function

Based on the facts and arguments presented in the previous section, the following depth-dependent function for c_f was developed:

$$c_f(x) = \begin{cases} C_{fo} & ;x \geq X_b/2 \\ C_{fo}\left(\dfrac{h(X_b/2)}{h(x)}\right) & ;x < X_b/2 \end{cases} \quad (45)$$

C_{f0} is a constant to be tuned by data, and X_b is surf zone width computed in the model. The function $c_f(x)$ is based on X_b, which is based on an optimal percent wave breaking threshold of 10 percent. Figure 7 shows that the empirical mean value of $x(/V/_{max})/X_b$ is approximately 0.40; however, a value of 0.50 is used in Eq. (46).

The variation of c_f inversely with depth is not completely arbitrary. First, there is preferential sorting of sediment types by grain size in the nearshore, with larger grain sizes in the intertidal zone and finer material offshore. Howd and Birkemeier (1987) and Birkemeier (1991) have shown that at Duck beach median grain size varies from 0.70 mm on the steep foreshore, to 0.20 mm over the bar, and 0.12 mm offshore. Second, Eq. (45) has a form similar to the effective depth-dependent functions used by Smith et al. (1993) and used by Garcez Faria et al. (1998).

The typical variation of the proposed c_f over a barred beach is shown in Fig. 8, which gives the depth and the associated function c_f for the 2200 EST 10 October 1990 DELILAH case. The edge of the surf zone at X_b = 128 m. The bottom friction $c_f(x) = C_{f0} = 0.003$ is constant to a distance of 64 m with depth h = 1.6 m. Shoreward of mid surf zone $X_b/2$, the depth increases and the bottom friction decreases to a minimum of c_f = 0.0024 at x = 41.2 m and h = 2.1 m. Bottom friction then increases linearly near the edge of the water to a maximum of c_f = 0.0141 at x = 3.4 m, h = 0.35 m. The model automatically terminates at the most shoreward grid point where the depth is greater than 0.5 ft (0.15 m). Thus, for depths greater than 0.15 m the bottom friction will never reach more than about ten times C_{f0} if $h(X_b/2)$, the depth at mid surf zone, is 1.5 m.

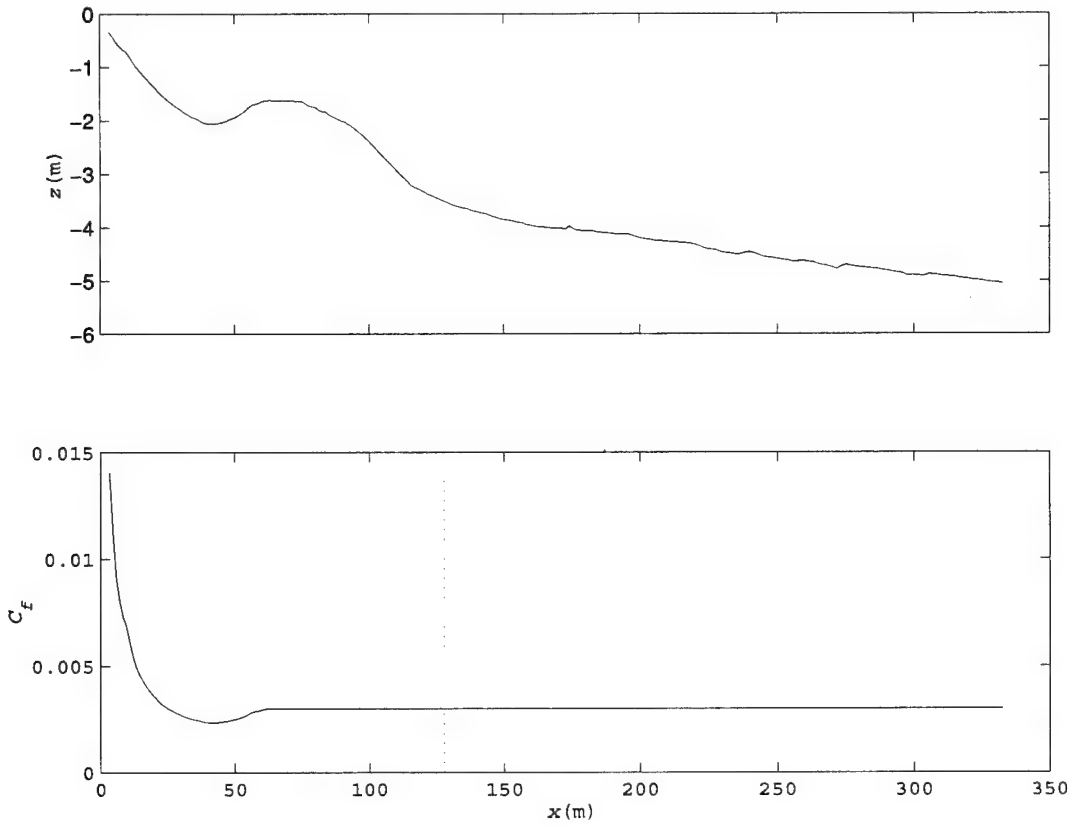

Fig. 8 — Profiles of depth (top) corrected for tide stage for DELILAH case 2200 EST,10 October 1990, and associated function c_f (bottom) using C_{f0} = 0.003. Surf zone width for this case is estimated by model to be 128 m.

5.2 Optimal C_{f0} and M

The basic formulation [Eq. (46)] yields significant improvements in the current if the proper value of C_{f0} and M is used. Because of the large data set available, various combinations of these two parameters are used in the model to produce estimates for each of the DELILAH and DUCK94 cases, which are then compared to measurements from which model skill is determined.

Before selecting optimal C_{f0} and M, it is useful to examine the effects of varying C_{f0} and M, as illustrated for a single DELILAH case in Fig. 9. It shows several current profiles from surf model runs for which C_{f0} or M is held constant, respectively. The increase of horizontal eddy viscosity causes more mixing and produces a less peaked longshore current profile. The mixing depends on the dissipation rate, therefore it has the strongest effect near the bar crest where dissipation rate is often highest. The parameter C_{f0} has a strong effect on the magnitude of the current throughout the whole surf zone.

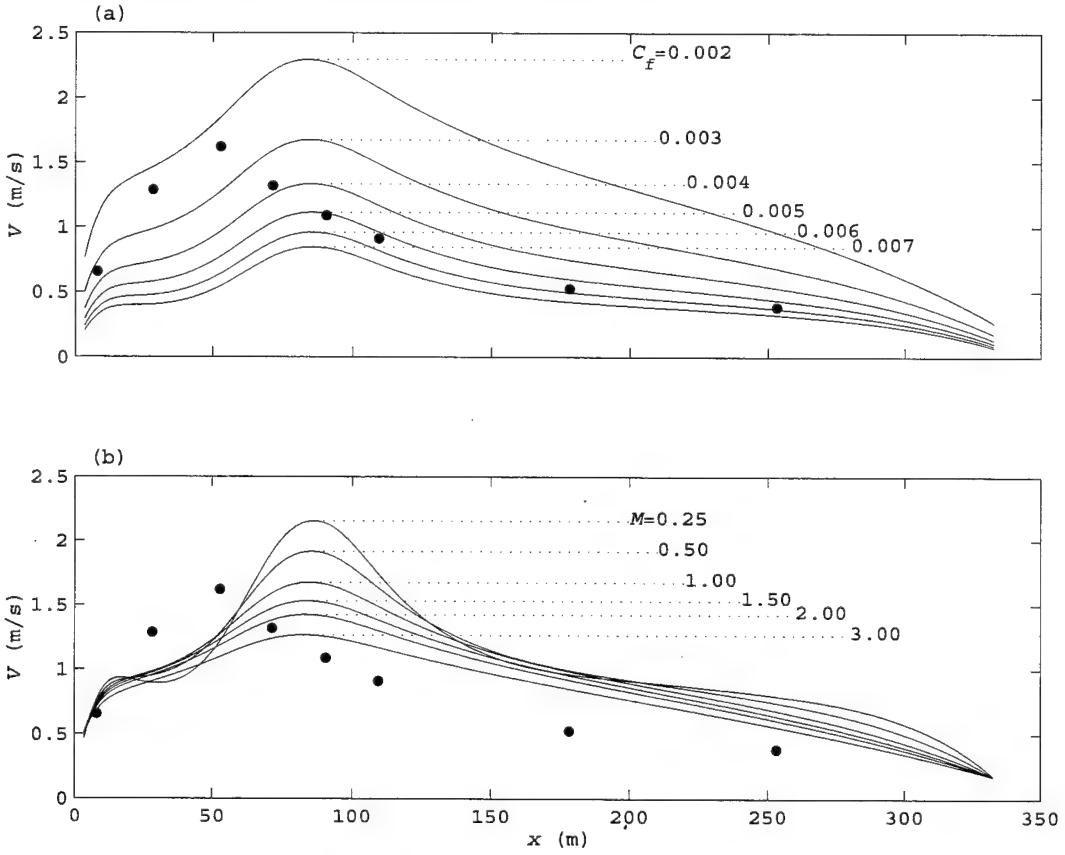

Fig. 9 — Profiles of longshore current V from SURF 3.0 with the addition of Eq. (45)—DELILAH, 10 October 1990, 2200 UTC. Surf zone measurements given by dots. (a) M =1.0 for all profiles, C_{f0} as noted; (b) C_{f0} = 0.003 for all profiles, M as noted

Both DELILAH and DUCK94 measurements are used to derive the optimal values of C_{f0} and M. The 79 DELILAH cases and 144 DUCK94 cases were selected on the basis of data availability. Only those times for which wind, wave, depth, tide, and validating surf zone current measurements existed were used, and all such cases were used. Sixteen sets of model runs were made using different combinations of C_{f0} and M parameters. Model skill for each set of runs is summarized in Table 2 in terms of various skill statistics. The results of SURF 3.0 using a fixed C_{f0} are listed at the bottom of the table. This case, along with the case of

Table 2 — Performance of longshore current estimates when using denoted C_{f0} in the variable function of $c_f(x)$ an M. Two minimum speeds (0.001 m/s and 0.1 m/s), below which dtaa are not included in computing the statistics, are used to reduce the effect of large number of data points at low current speeds. Bottom row shows the results from the old model with constant c_f.

***For* τ = 0.001 m/s**

C_{f0}	M	ε_{min}	ε_{mean}	$\varepsilon_{mean\text{-}abs}$	ε_{max}	σ	R	ε_{100}	ε_{100abs}	m	b	N
0.00225	1.00	-1.31	-0.17	0.24	1.18	0.28	0.89	12.20	165.27	1.15	-0.18	1922
0.00225	1.50	-1.13	-0.17	0.23	1.09	0.25	0.89	2.85	159.49	1.07	-0.17	1922
0.00225	1.75	-1.06	-0.16	0.22	1.04	0.24	0.89	-1.08	156.78	1.04	-0.17	1926
0.00225	3.00	-0.93	-0.16	0.21	0.87	0.21	0.89	-15.38	147.32	0.91	-0.15	1922
0.00250	2.00	-0.97	-0.15	0.21	0.92	0.21	0.89	-11.53	142.55	0.93	-0.15	1922
0.00300	**1.00**	**-1.06**	**-0.14**	**0.20**	**0.91**	**0.22**	**0.89**	**-11.50**	**129.65**	**0.89**	**-0.14**	**1926**
0.00300	1.40	-1.04	-0.14	0.19	0.86	0.21	0.89	-16.65	127.59	0.85	-0.13	1922
0.00300	2.00	-1.03	-0.14	0.19	0.80	0.20	0.89	-22.86	125.00	0.80	-0.13	1922
0.00350	0.75	-1.06	-0.13	0.19	0.70	0.21	0.89	-31.58	113.66	0.71	-0.11	1926
0.00350	0.80	-1.15	-0.16	0.24	0.83	0.27	0.82	-54.04	129.93	0.57	-0.14	1922
0.00350	1.00	-1.09	-0.13	0.19	0.79	0.21	0.88	-22.26	116.55	0.77	-0.12	1926
0.00350	2.00	-1.11	-0.13	0.19	0.81	0.22	0.88	-19.02	117.89	0.79	-0.12	1926
0.00400	0.60	-1.13	-0.12	0.19	0.71	0.23	0.87	-25.91	109.74	0.71	-0.10	1922
0.00400	0.70	-1.13	-0.12	0.19	0.70	0.23	0.87	-27.22	109.13	0.70	-0.10	1922
0.00400	0.75	-1.13	-0.12	0.19	0.70	0.22	0.87	-27.83	108.88	0.70	-0.10	1922
0.00400	0.80	-1.12	-0.12	0.19	0.70	0.22	0.87	-28.42	108.65	0.70	-0.10	1922
0.00400	0.90	-1.12	-0.12	0.19	0.69	0.22	0.88	-29.52	108.26	0.69	-0.10	1922
0.00400	1.00	-1.12	-0.12	0.19	0.69	0.22	0.88	-30.54	107.95	0.69	-0.10	1922
0.00700	**2.00**	**-1.15**	**-0.10**	**0.22**	**0.57**	**0.27**	**0.87**	**-49.90**	**97.47**	**0.48**	**-0.07**	**1922**

***For* τ = 0.1 m/s**

C_{f0}	M	ε_{min}	ε_{mean}	$\varepsilon_{mean\text{-}abs}$	ε_{max}	σ	R	ε_{100}	ε_{100abs}	m	b	N
0.00225	1.00	-1.31	-0.20	0.27	1.10	0.28	0.90	6.77	72.78	1.15	-0.21	1582
0.00225	1.50	-1.13	-0.19	0.25	0.90	0.25	0.91	-0.08	69.14	1.08	-0.20	1582
0.00225	1.75	-1.06	-0.19	0.25	0.84	0.24	0.91	-3.16	67.74	1.05	-0.20	1585
0.00225	3.00	-0.93	-0.18	0.23	0.61	0.21	0.91	-14.97	63.17	0.91	-0.18	1582
0.00250	2.00	-0.97	-0.18	0.23	0.66	0.22	0.91	-13.28	62.40	0.94	-0.18	1582
0.00300	**1.00**	**-1.06**	**-0.17**	**0.22**	**0.67**	**0.22**	**0.90**	**-17.05**	**59.44**	**0.90**	**-0.16**	**1585**
0.00300	1.40	-1.04	-0.17	0.22	0.56	0.21	0.90	-20.48	58.33	0.86	-0.16	1582
0.00300	2.00	-1.03	-0.16	0.21	0.47	0.21	0.91	-25.06	57.38	0.81	-0.15	1582
0.00350	0.75	-1.06	-0.15	0.21	0.48	0.22	0.91	-34.04	55.54	0.71	-0.13	1585
0.00350	0.80	-1.15	-0.19	0.27	0.55	0.28	0.84	-45.76	68.19	0.57	-0.16	1582
0.00350	1.00	-1.09	-0.15	0.21	0.48	0.22	0.90	-27.75	56.23	0.78	-0.14	1585
0.00350	2.00	-1.11	-0.15	0.22	0.57	0.23	0.89	-25.94	56.96	0.80	-0.14	1585
0.00400	0.60	-1.13	-0.14	0.22	0.48	0.24	0.88	-33.66	55.97	0.71	-0.12	1582
0.00400	0.70	-1.13	-0.14	0.22	0.48	0.24	0.88	-34.24	55.60	0.71	-0.12	1582
0.00400	0.75	-1.13	-0.14	0.22	0.48	0.24	0.89	-34.53	55.46	0.70	-0.12	1582
0.00400	0.80	-1.12	-0.14	0.21	0.48	0.24	0.89	-34.81	55.34	0.70	-0.12	1582
0.00400	0.90	-1.12	-0.14	0.21	0.48	0.23	0.89	-35.38	55.17	0.70	-0.12	1582
0.00400	1.00	-1.12	-0.14	0.21	0.48	0.23	0.89	-35.94	55.07	0.69	-0.12	1582
0.00700	**2.00**	**-1.15**	**-0.12**	**0.25**	**0.57**	**0.29**	**0.88**	**-52.55**	**60.85**	**0.48**	**-0.09**	**1582**

C_{f0} = constant factor in the function c_f
M = coefficient used in lateral mixing ν_t
ε_{min} = minimum error (m/s)
ε_{mean} = simple mean of the individual errors (model - measurement) (m/s)
$\varepsilon_{mean\text{-}abs}$ = mean of absolute value of errors (below ε_{mean})
ε_{max} = maximum error (m/s)
σ = standard deviation of the error (± m/s)
R = linear correlation coefficient between mode estimates and measurements
ε_{100} = 100 × mean fractional effor ([model-meas.]/meas.; meas. ≠ 0)
ε_{100abs} = 100 × mean absolute value of fractional error
m = slope of regression line through model-measurement pairs
b = y-intercept. Offset of regression line through model-measurement pairs (m/s)
N = number of model-measurement pairs

C_{f0} = 0.003 and M = 1.0 are in bold font for easy comparison. It should be noted that large numbers of low and near-zero current speeds can contribute high relative and percentage errors. In Table 2, two minimum speeds (0.001 m/s and 0.1 m/s), below which the data are not included, are used. Under the higher minimum speed, the total number of points drops from 1922 to 1582. Except the relative errors, most of the statistics do not vary much. It is evident that decreasing C_{f0} in general produces better statistics. Among several best available combinations, C_{f0} = 0.003 and M = 1.0 were selected because of its lower ε_{100} and standard deviation values. Comparing to SURF 3.0, the ε_{100} error of the improved model has reduced to 17.5 from 52.3%. The slope of the linear regression curve has also improved from 0.48 to 0.89.

From the preceding analysis of model errors, summarized in Table 2, the optimal values C_{f0} = 0.003 and M = 1.0 are used for the cases studies presented in the remainder of this report. The value of C_{f0} = 0.003 is found to be close to those values used in the recent literature.

5.3 Scatter Plots

Figure 10 is a plot of 1930 measurements vs improved model estimates using the optimal bottom friction and horizontal mixing coefficients. (Skill statistics in the figure are defined the same as in Table 2.) Compared to Fig. 4, the improved model achieves significant improvement for a current larger than 0.5 m/s. The improvement is also evident from the slope of the linear regression line changing from 0.48 to 0.89.

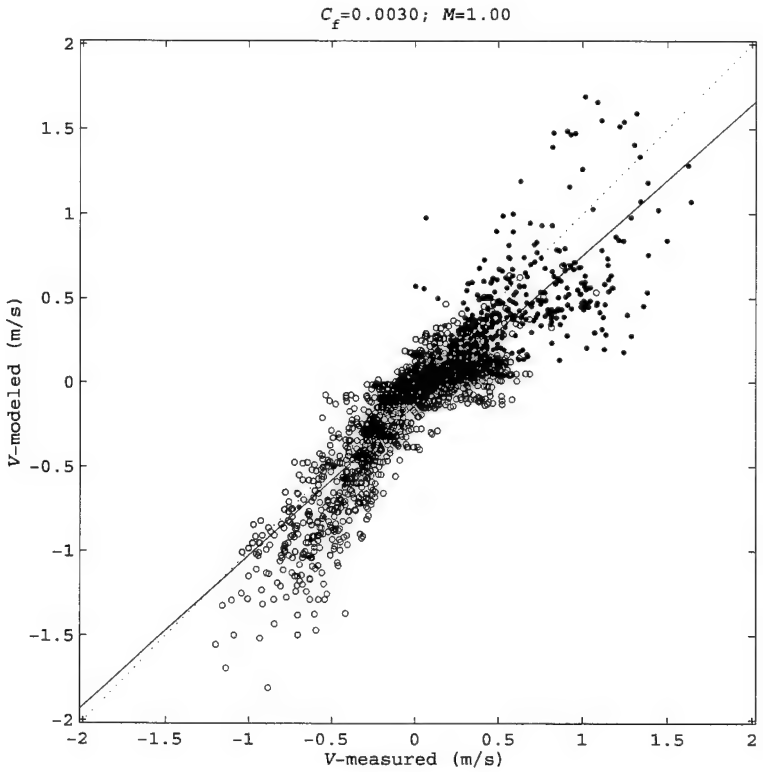

Fig. 10 — Scatter diagram of measured longshore currents vs the corresponding improved model estimates of current. Dots denote DELILAH measurements; circles denote DUCK94 measurements. N = 1930 observations. Skill statistics based on model minus measured differences of set from combined data sets are: linear correlation coefficient R = 0.89; minimum error ε_{min} = –1.06 m/s; mean error ε_{mean} = –0.14 m/s; maximum error ε_{max} = 0.91 m/s; standard deviation of the errors σ = 0.22 m/s. The solid line is a linear regression curve with slope m = 0.89 and y-intercept b = –0.14 m/s.

As stated before, the accuracy of the model in estimating the maximum current in the surf zone is very important with regard to modified surf index (MSI) computations, for which only the maximum current in the surf zone is used. The maximum longshore current from the two data sets is given in Fig.11, which can be readily compared to Fig. 5. There is a significant improvement in estimates of V_{max}; the root-mean-square error decreases from 0.32 m/s to 0.27 m/s, and the mean fraction error decreases from –40 to –30 percent. As previously mentioned, the statistical improvement should be a lot better if SURF 3.0 excludes those cases where V_{max} occurs near water edge rather than at mid surf zone.

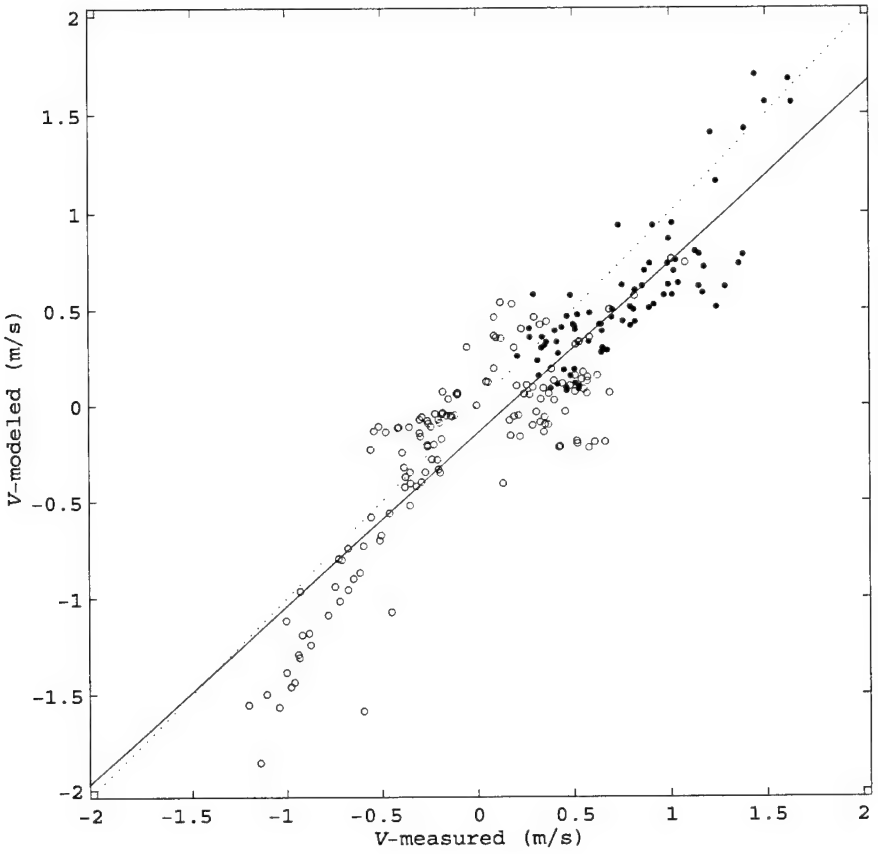

Fig. 11 — Scatter diagram of maximum longshore current measurement within surf zone to corresponding improved model-estimated longshore current. Dots denote DELILAH measurements; circles denote DUCK94 measurements. $N = 223$ observations. Skill statistics based on model minus measured differences of set from combined data sets are: linear correlation coefficient $R = 0.899$; minimum error $\varepsilon_{min} = -0.99$ m/s; mean error $\varepsilon_{mean} = -0.17$ m/s; maximum error $\varepsilon_{max} = 0.41$ m/s; standard deviation of the errors $\sigma = 0.27$ m/s. The solid line is a linear regression curve with slope $m = 0.89$ and y-intercept $b = -0.15$ m/s.

6.0 ADDITIONAL RESULTS

In this section, the effectiveness of our new function and empirically selected C_{f0} and M is shown, using measurements acquired from NSTS, DELILAH, and DUCK94. The four NSTS cases are used to validate the improved model because no data were used in selecting C_{f0} and M. This section also presents several cases studies from the respective DELILAH and DUCK94 data sets.

6.1 Validation Using NSTS Santa Barbara Data

Results from four cases from the NSTS at Leadbetter Beach, Santa Barbara, California, in February 1980 are presented next. In this, and the two following sections, model results from SURF 3.0 with and without the improved bottom friction function and viscosity parameter are examined. The improved version was run using $C_{f0} = 0.003$ and $M = 1.0$.

Figures 12-15 give cross-shore profiles of depth, root-mean-square wave height, the percentage of breaking waves, and longshore current. In each figure, circles denote measurement locations or measured data. In these four figures and in similar figures in Sections 6.3 and 6.4, which give individual cases from DELILAH and DUCK94, the edge of the surf zone is denoted as a dotted vertical line in the third panel. This is the location where the percentage of breaking waves is estimated to reach 10 percent. Relevant offshore wave parameters used for model initialization are noted on each figure beneath the top panel.

Thornton and Guza (1986) used the four cases in this section to validate a precursor to the model used in SURF 3.0. Earle (1989) used three of the four cases to validate the first version of the NSSM based on Thornton and Guza (1986). These are ideal cases. First, the nearshore depth contours during the experiment were nearly straight and parallel to the beach. Secondly, the offshore waves consisted mainly of swells with narrow banded frequency and direction.

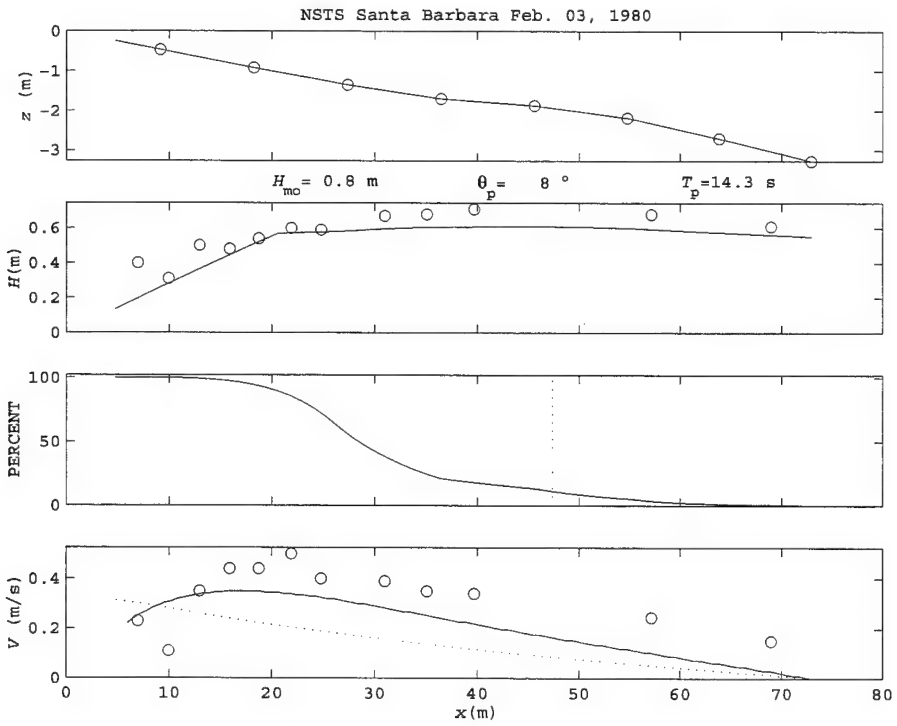

Fig. 12 — NSTS planar beach, 3 February 1980. Profiles of surf zone parameters: depth; root-mean-square wave height; percent breaking or broken waves; longshore current, standard model (dotted) and improved model (solid). Improved model estimates based on C_{f0} = 0.003 and M = 1.0.

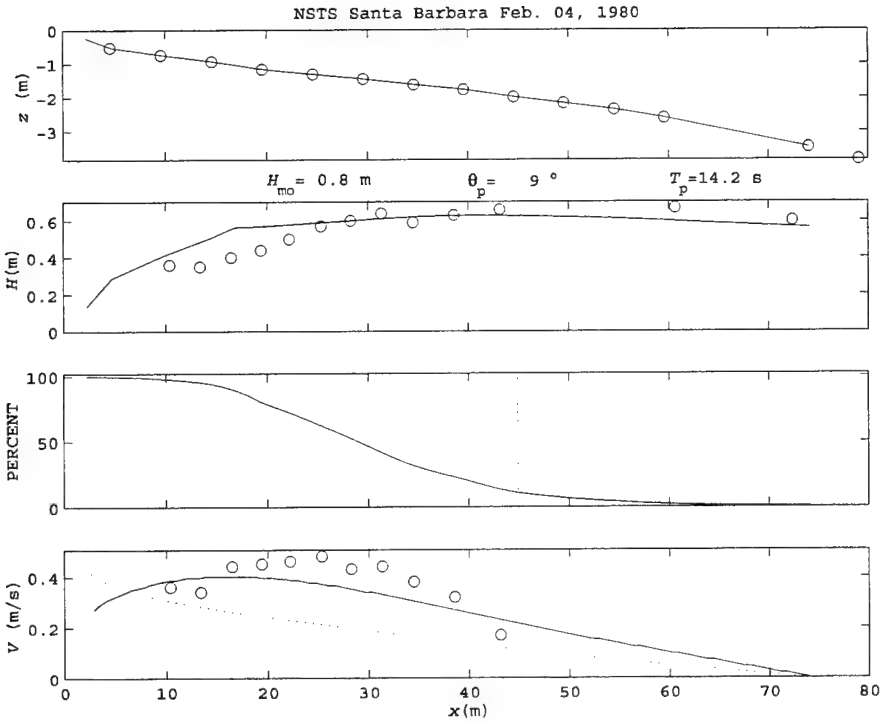

Fig. 13 — NSTS planar beach, 4 February 1980. Profiles of surf zone parameters: depth; root-mean-square wave height; percent breaking or broken waves; longshore current, standard model (dotted) and improved model (solid). Improved model estimates based on C_{f0} = 0.003 and M = 1.0.

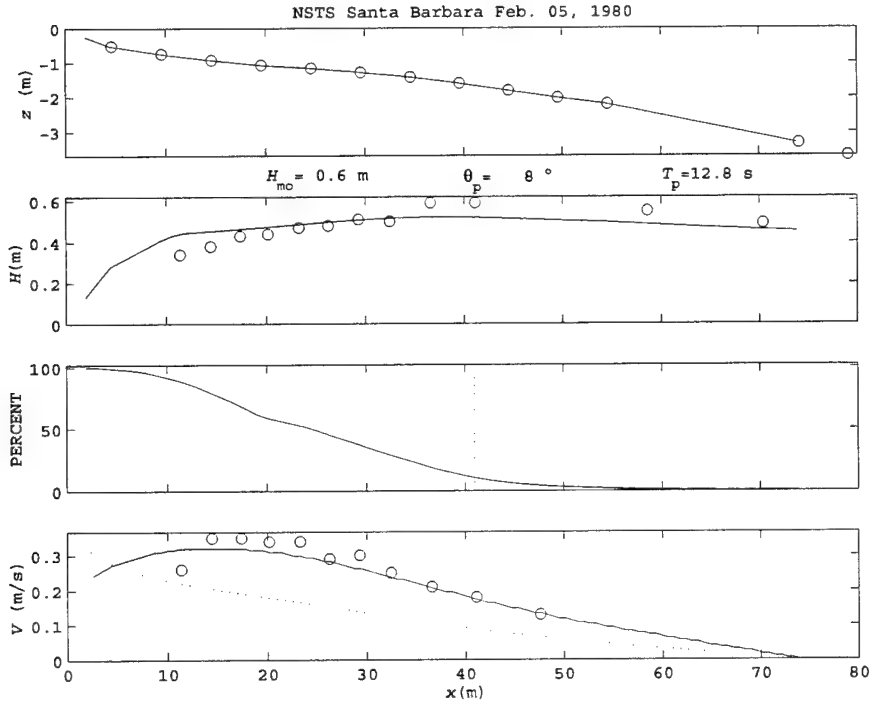

Fig. 14 — NSTS planar beach, 5 February 1980. Profiles of surf zone parameters: depth; root-mean-square wave height; percent breaking or broken waves; longshore current, standard model (dotted) and improved model (solid). Improved model estimates based on C_{f0} = 0.003 and M = 1.0.

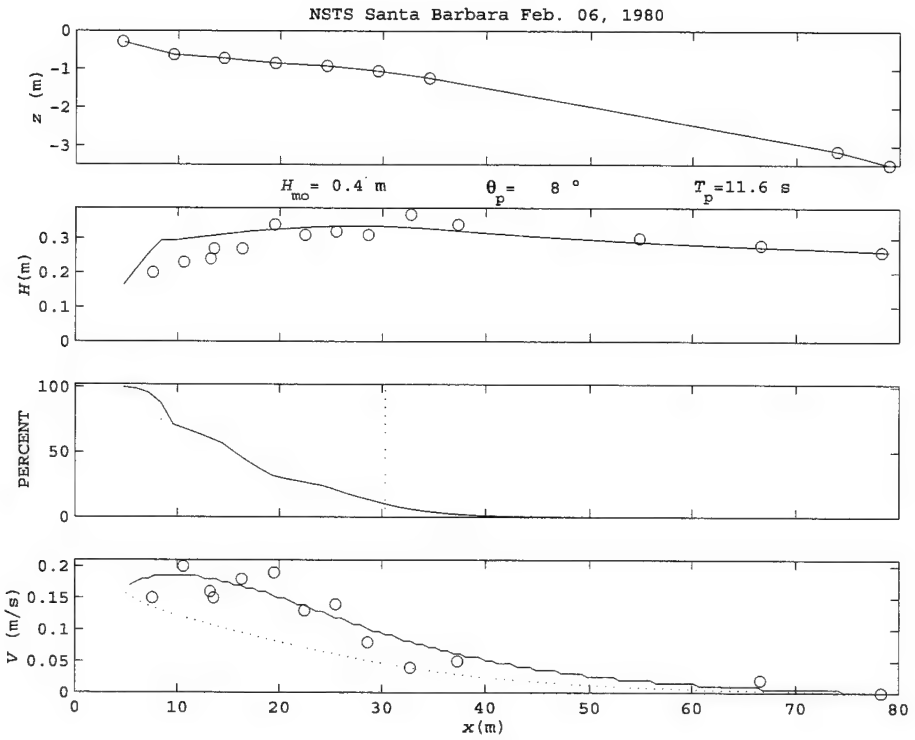

Fig. 15 — NSTS planar beach, 6 February 1980. Profiles of surf zone parameters: depth; root-mean-square wave height; percent breaking or broken waves; longshore current, standard model (dotted) and improved model (solid). Improved model are based on $C_{f0} = 0.003$ and $M = 1.0$.

Of importance, Santa Barbara data have not been used in model calibration in choosing the bottom friction and eddy viscosity, so it is indeed encouraging that the improved model produces excellent results compared to SURF 3.0. In all four cases, the improved model reaches a peak that is closer in space to the observed peak than is the peak in SURF 3.0. The shape of the profile from the improved model compares relatively well to the shape of the measured profile.

6.2 DELILAH Cases

Figures 16-20 are plots for five DELILAH cases from 8 to 12 October 1990. The location of pressure gages (+'s) and current meters (o's) are denoted in the first panel of each figure. The same symbols are used to denote respective measured data in panels 2 and 4. Tide, wind speed, and direction are also listed under the first panel. Wave parameters from the directional wave spectra acquired at an 8-m-deep array of pressure gages 0.5 nmi offshore and used as input to surf model are listed under the second panel. Validating wave height and longshore current measurements are averaged over the same time duration as the 136-min time duration during which the wave spectra were acquired.

Figures 16 and 17 represent low longshore current cases with no obvious bar feature on the beach profile. The new model shows a significant improvement in longshore current prediction. It is typical that the old model, as in Fig. 17, shows a monotonic increasing longshore current toward the beach with a high tide. The new variable bottom friction function has eliminated this incorrect trend. Figures 18 and 19 represent high longshore currents over a barred beach. These days are also selected because the wave heights are near the critical value for some amphibious operations. The new model is again proven significantly better in estimating the maximum current. It also eliminates the second peak near the beach. Figure 20 shows a case of low current over a barred beach. Compared to the old model, the location of the maximum current is significantly improved.

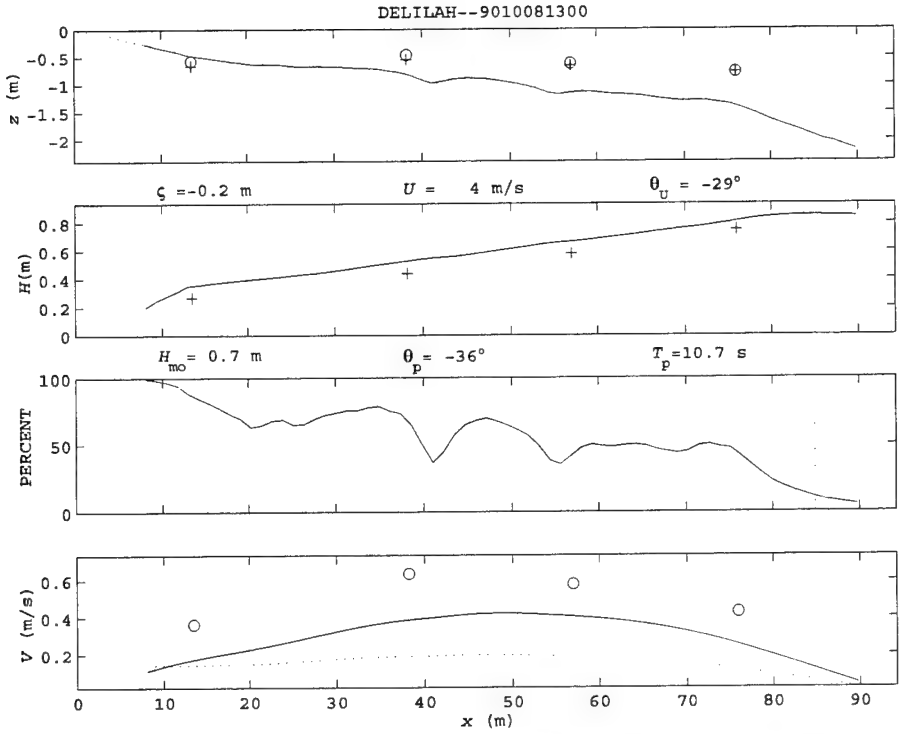

Fig. 16 — DELILAH beach, 1300 EST, 8 October 1990. Profiles of surf zone parameters: depth; root-mean-square wave height; percent breaking or broken waves; longshore current, standard model (dotted) and improved model (solid). Improved model estimates based on $C_{f0} = 0.003$ and $M = 1.0$.

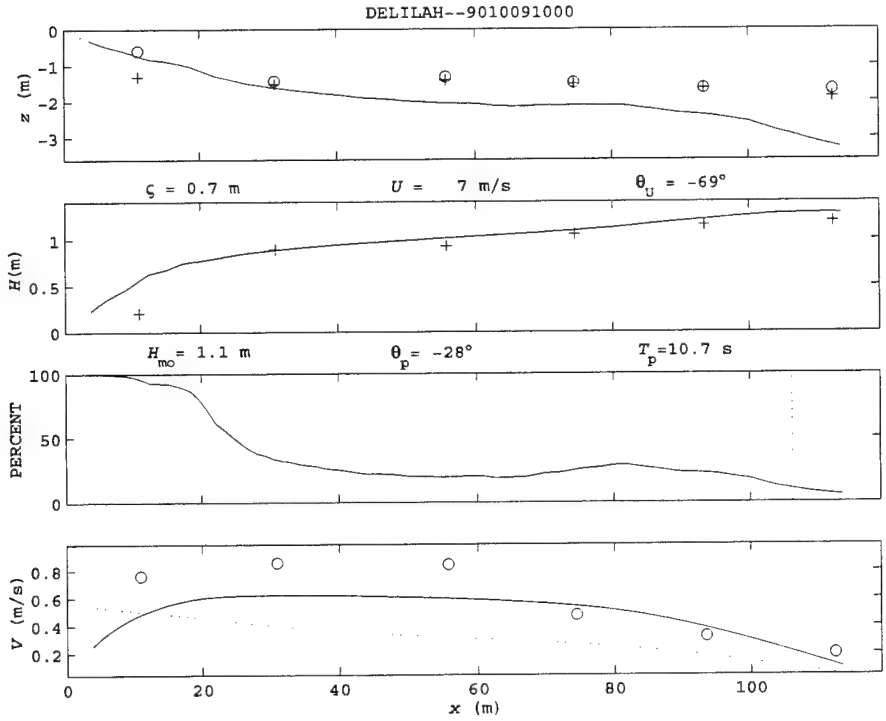

Fig. 17 — DELILAH beach, 1000 EST, 9 October 1990. Profiles of surf zone parameters: depth; root-mean-square wave height; percent breaking or broken waves; longshore current, standard model (dotted) and improved model (solid). Improved model estimates based on $C_{f0} = 0.003$ and $M = 1.0$.

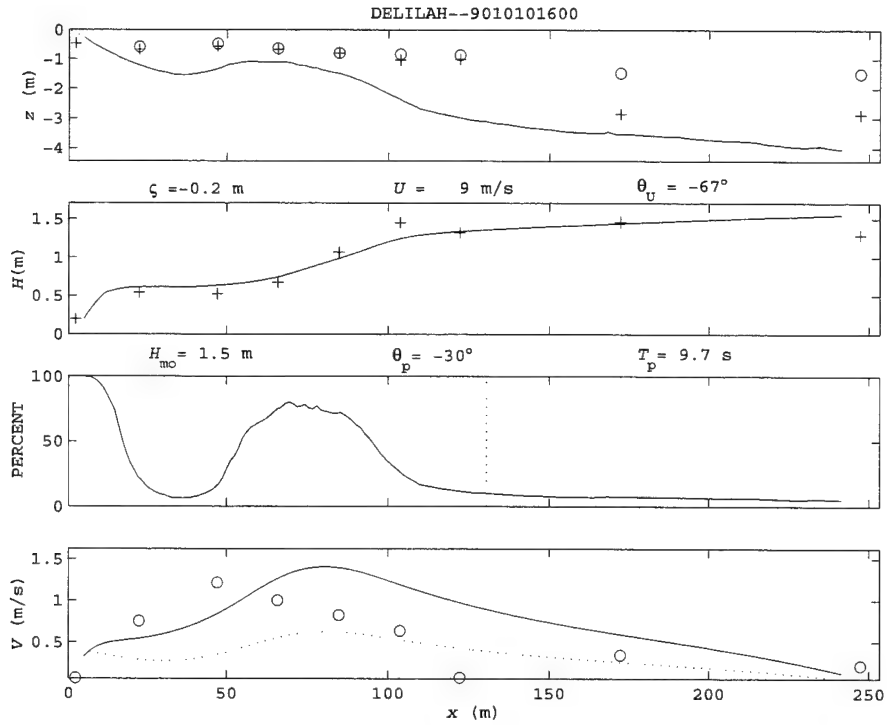

Fig. 18 — DELILAH barred beach, 1600 EST, 10 October 1990. Profiles of surf zone parameters: depth; root-mean-square wave height; percent breaking or broken waves; longshore current, standard model (dotted) and improved model (solid). Improved model estimates based on $C_{f0} = 0.003$ and $M = 1.0$.

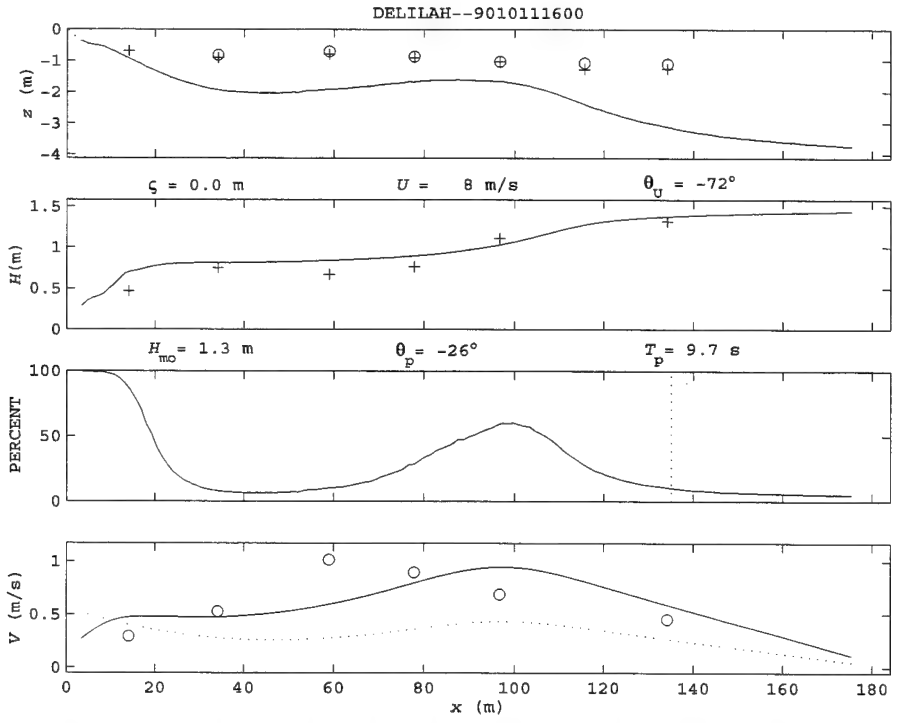

Fig. 19 — DELILAH barred beach, 1600 EST, 11 October 1990. Profiles of surf zone parameters: depth; root-mean-square wave height; percent breaking or broken waves; longshore current, standard model (dotted) and improved model (solid). Improved model estimates based on $C_{f0} = 0.003$ and $M = 1.0$.

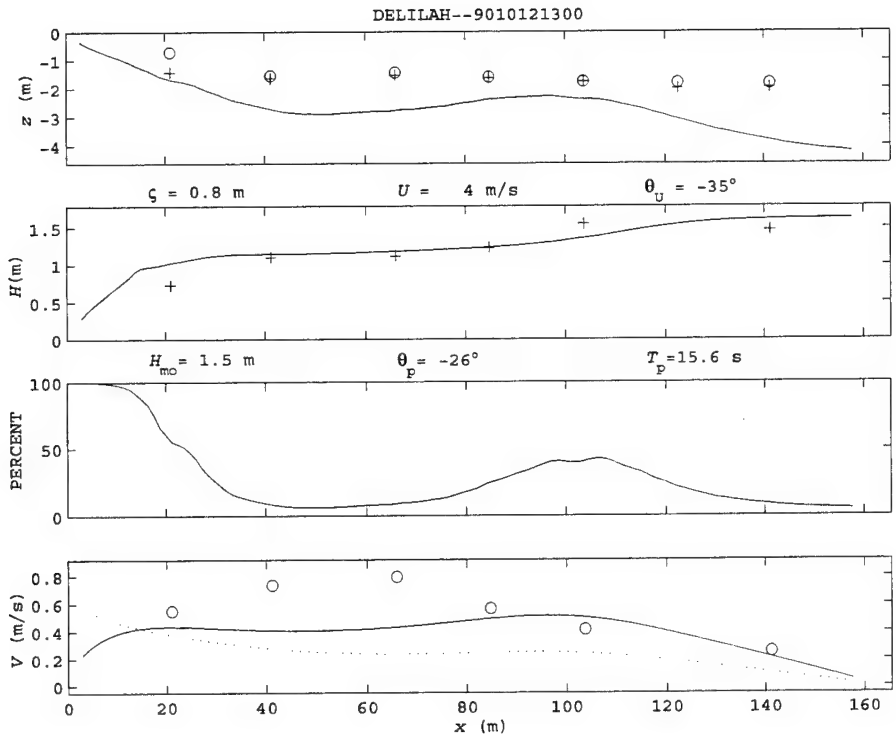

Fig. 20 — DELILAH barred beach, 1300 EST, 12 October 1990. Profiles of surf zone parameters: depth; root-mean-square wave height; percent breaking or broken waves; longshore current, standard model (dotted) and improved model (solid). Improved model estimates based on $C_{f0} = 0.003$ and $M = 1.0$.

For all cases, including Eq. (46) in the model improves the overall accuracy of the estimated current profile, especially the maximum current in the surf zone. In all cases however, the location of the measured current maximum is shoreward of that estimated by the model. It has been a characteristic of the DELILAH data set that the maximum longshore current occurs over the trough shoreward of the bar crest. But the computed maximum occurs over the crest of the bar, where there is a sharp increase in wave breaking and energy dissipation. Much research by the writers and others has been devoted to resolving this discrepancy. This issue is additionally discussed later.

6.3 DUCK94 Cases

Figures 21-24 present model and data comparisons selected from four different days (October 10-13) of the DUCK94 experiment. Waves were coming from northeast for October 10-12, and turned to be from the southeast on October 13. Data from October 10-12 were chosen because of the strong longshore current and also because field observations of bed shear stresses are available (Garcez Faria et al., 1998). October 13 is selected to provide an example for a current flowing in an opposite direction. Perhaps the most important difference between first three examples and the DELILAH cases is that the wave forcing is from the northeast rather than from the southeast. Thus, there is no chance that current forcing is perturbed by the presence of the FRF pier and the deep scour hole below it, which is located south of the surf observation area. During all four days, bar features exist on all beach profiles.

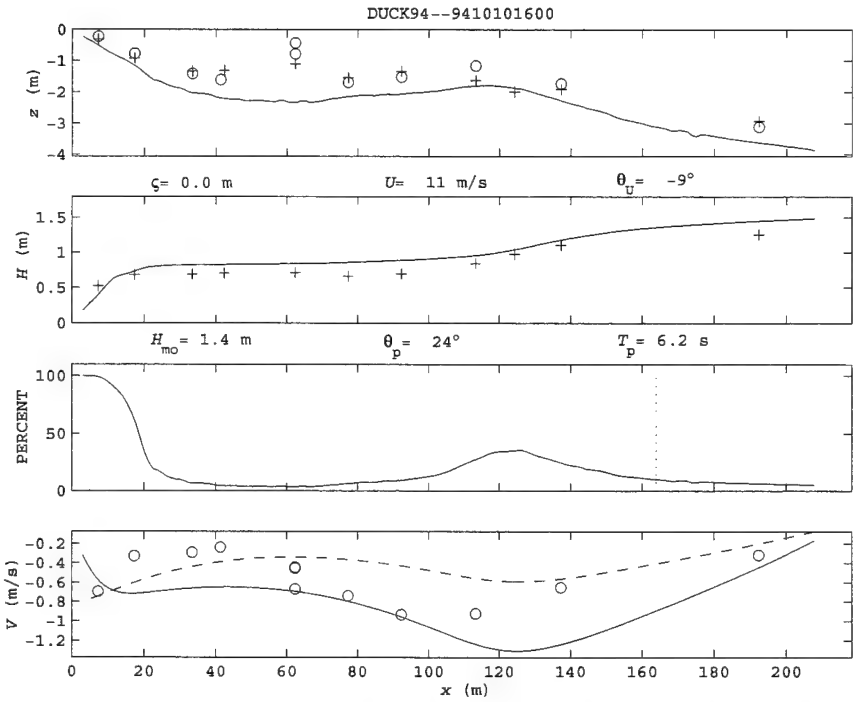

Fig. 21 — DUCK94 barred beach, 1600 EST, 10 October 1994. Profiles of surf zone parameters: depth; root-mean-square wave height; percent breaking or broken waves; longshore current, standard model (dotted) and improved model (solid). Improved model estimates based on $C_{f0} = 0.003$ and $M = 1.0$.

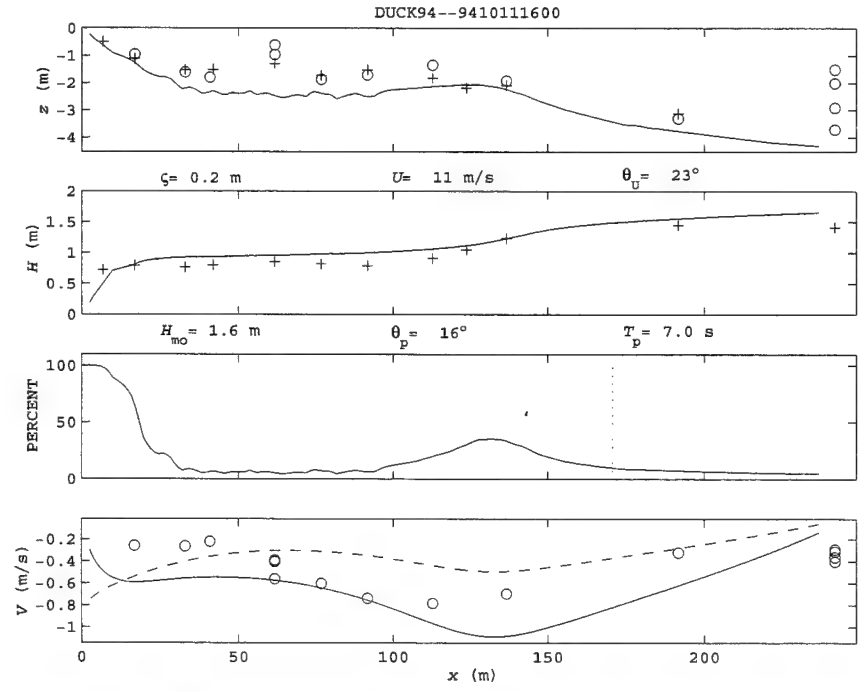

Fig. 22 — DUCK94 barred beach, 1600 EST, 11 October 1994. Profiles of surf zone parameters: depth; root-mean-square wave height; percent breaking or broken waves; longshore current, standard model (dotted) and improved model (solid). Improved model estimates based on $C_{f0} = 0.003$ and $M = 1.0$.

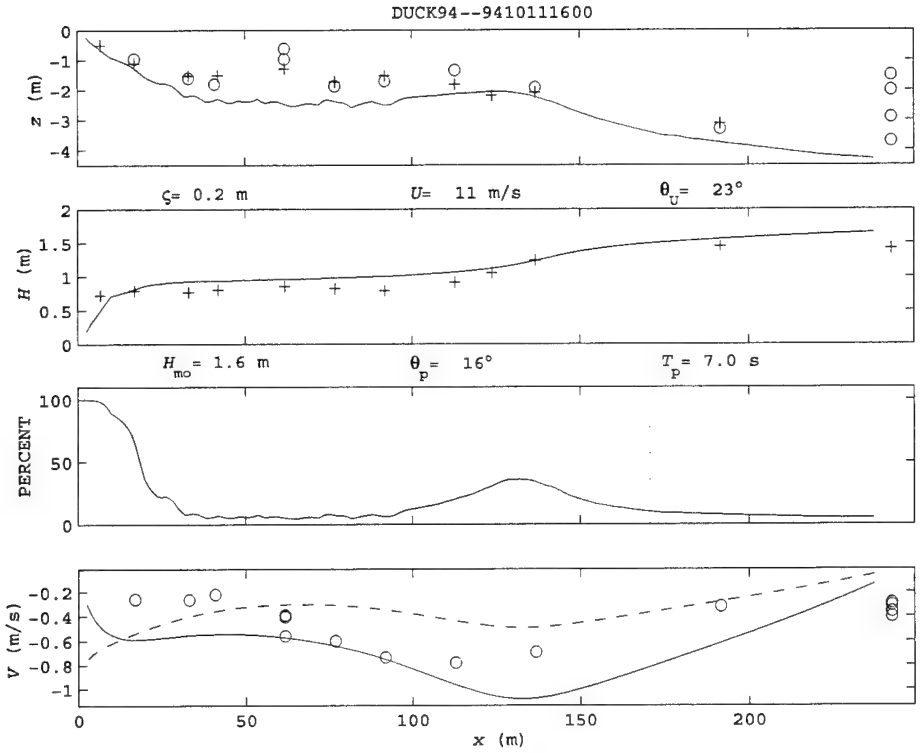

Fig. 23 — DUCK94 barred beach, 1300 EST, 12 October 1994. Profiles of surf zone parameters: depth; root-mean-square wave height; percent breaking or broken waves; longshore current, standard model (dotted) and improved model (solid). Improved model estimates based on $C_{f0} = 0.003$ and $M = 1.0$.

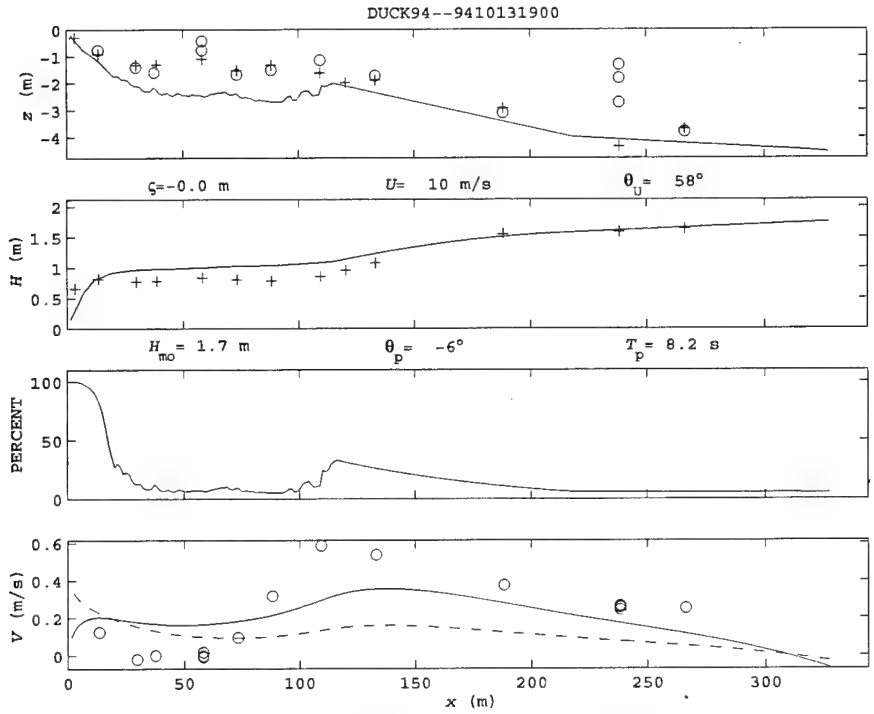

Fig. 24 — DUCK94 barred beach, 1900 EST, 13 October 1994. Profiles of surf zone parameters: depth; root-mean-square wave height; percent breaking or broken waves; longshore current, standard model (dotted) and improved model (solid). Improved model estimates based on $C_{f0} = 0.003$ and $M = 1.0$.

Figures 21 and 22 (October 10 and 11) have similar wave and wind conditions. The improved model overpredicts the maximum current slightly, but the unrealistic second peak near the beach from the old model is significantly reduced. Figure 23 (October 12) represents a high wave event with significant wave height of 2.3 m and wind speed of 14 m/s. Even with higher waves, the longshore current is smaller than on October 10-11 due to smaller wave angle relative to beach normal. The measured current peak moves further into the trough. In Fig. 24 (October 13), the wave direction is coming from the southeast and the wind has decreased to 10 m/s. Although the new model does not produce a maximum longshore current as high as measured, the maximum from the new model is twice that of the old model.

In general, Figs. 21-24 show that the improved model provides better longshore current estimates than the old model. Although there is a gradual decrease in the magnitude of the computed current over the most shoreward quarter of the surf zone, measured current shows much sharper decrease. This suggests that, for the last quarter of the beach, flow resistance begins earlier and at a higher magnitude than that which can be controlled by the improved bottom friction function. Other flow resistance mechanisms such as surf zone turbulence, i.e., the turbulent Reynolds stress, may play an important role. The turbulence from breaking waves may effectively retard mean current motion due to vertical shearing stress that is not treated in one-dimensional models. It should be pointed out that the ratio of turbulence penetration depth to local depth is relatively large at very shallow depth, making this omission more serious.

7.0 DISCUSSION

This section discusses three important aspects of the improved longshore current model. First, the difference between horizontal eddy viscosity values used in our one-dimensional (1D) and another quasi-3D model is discussed. Next, our new bottom friction function is compared with field measurement. Finally, the location of the longshore current maximum is discussed.

7.1 Lateral Eddy Viscosity

In our model, the turbulent eddy viscosity is based on Battjes' (1975) formulation as shown as Eq. (25). His formulation has been widely used by nearshore hydrodynamic models. The empirical constant M is generally thought to be of order one. Based on laboratory data, Battjes (1983) showed that M is equal to 0.8. A wide range of M values from 0.025 to 2 has been used by different models. The optimal value we derive is 1.0 whereas SURF 3.0 uses 2.0. In a recent development of the quasi-3D SHORECIRC model, Sancho (1999) used an M value of 0.1, which is an order of magnitude smaller than ours. There are at least two reasons that we need to use a larger value. First, we need to compensate for the limitation of our 1D model in not including the nonlinear interactions between cross-shore and longshore currents. This mean flow interaction acts as an additional dispersive mechanism (Svendsen and Putrevu, 1994). Second, our 1D model includes only lateral or horizontal diffusion through ν_{tx} but not the vertical diffusion, i.e., ν_{tz}. On the other hand, SHORECIRC considers both eddy diffusions.

7.2 Bottom Friction Function

It is useful to compare our bottom friction function with field measurements. During DUCK94, current profiles were measured using a specially designed sled. Twenty-two vertical longshore current profiles were taken during the daylight hours of October 10-12. For the bottom boundary layer, logarithmic profiles were fitted to the data based on a least-squares method. c_f values were then derived from the slope of the least-square fit. These derived c_f values are listed in Garcez Faria (1997).

In Fig. 25, daylight hour profiles of our c_f and the derived values are plotted. The cross-shore distances given in Garcez Faria (1997) are converted to our convention, which is that zero is the edge of the water based on the depth profile and tide level. We do not know the exact time of each sled run; therefore, measured c_f values are plotted as an error bar indicating the uncertainty of the cross-shore distance due to the tide stage.

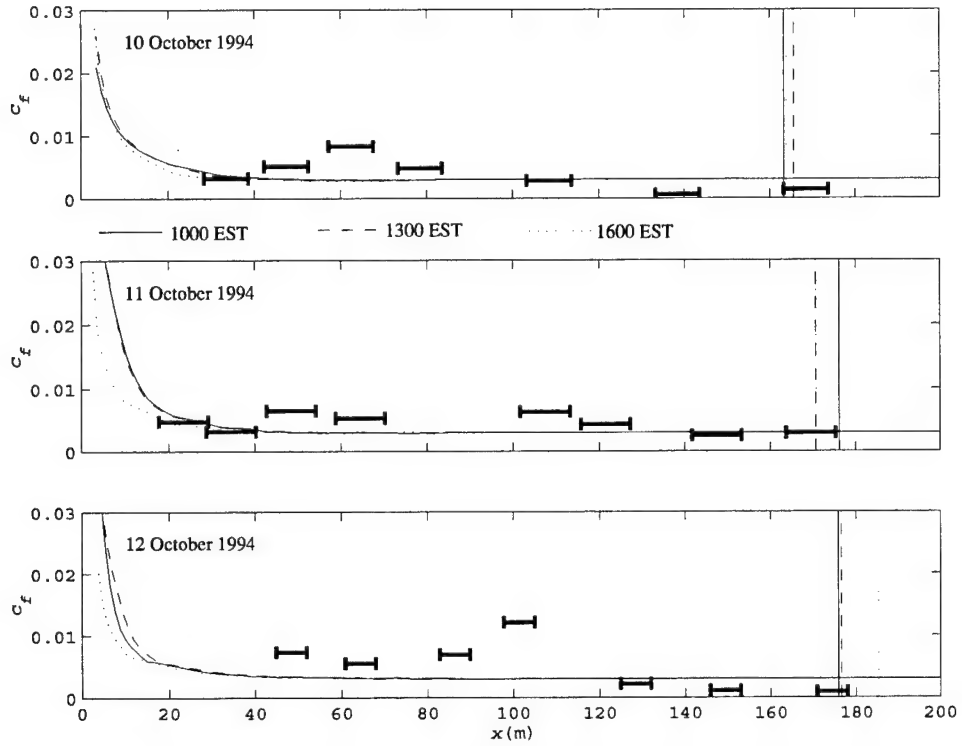

Fig. 25 — DUCK94, Comparison of c_f from Eq. (46) and measured data by Garcez Faria (1997) (heavy lines give the cross-shore range of the measured bottom friction coefficient; vertical lines denote esimated surf zone width for the respective case)

It is encouraging to see that our chosen value 0.003 for C_{f0} over the more seaward half of the surf zone is near the average values of measured bottom friction coefficeients. This value is not inconsistent to the 1986 Duck measurements of Whitford and Thorton (1996). They reported that mean bottom friction coefficient are 0.004, 0.003, and 0.001 for offshore the bar, on top and immediately in front of the bar, and in the trough. As shown in Fig. 25, our friction function does not catch the rise of c_f soon enough shoreward of the current peak over the shoreward-half of the surf zone. Also, the data from Garcez Faria show a fall of c_f values towards shore, but no current profiles farther near shore were taken to validate our assumption that bottom friction increases in very shallow water. The lack of observations at such depths is likely due to the technical difficulties in placing sensors in such very shallow water. In very shallow water, the penetration of breaking wave occupies most of the water column, making the logarithmic bottom boundary layer hard to define and measure. Thus, the characteristics of c_f in very shallow water are not well known.

There are reasons that justify our proposed rise in c_f near the water edge. First, it is well known that there is a general increase in the sand size from seaward to the water's edge, especially in the intertidal zone. The rise in our c_f in very shallow water accounts for this trend in bed roughness. Second, our higher values of c_f toward the water's edge partly compensate for the missing vertical mixing of our 1D model as discussed in Section 7.1.

There are other possibilities of choosing the variable in Eq. (46) rather than the depth, e.g., the percentage of breaking or wave height. After testing several parameters, the depth turns out to be the most robust choice. It is well known that the breaker height is proportional to depth in the saturated surf zone due to the depth-induced breaking. Therefore, the ratio between depths in Eq. (46) is equivalent to wave height ratio in the very shallow water. This may be the major reason why the variable friction function is successful in compensating the missing vertical mixing.

7.3 Location of Longshore Current Maximum

As mentioned, maximum measured longshore current often occurs in the trough of a barred beach. On the other hand, the maximum gradient of radiation stress from our model and others is always located over the bar crest. The shallow depth at the bar crest causes an increase of depth-induced wave breaking, thus producing a local current maximum near same location. Many research efforts have investigated this discrepancy. Using a large wave tank and a barred bottom, Reniers and Battjes (1997) found that the longshore current peak was located over the bar, which agrees with radiation stress theory. They concluded that the occurrence of the maximum longshore current velocities in the trough, as observed during DELILAH, is not the result of pure local wave forcing. However, these laboratory results must be framed within the context of length scale before applying them to field scenarios. Smith et al. (1993) suggested that the spatial lag between production and dissipation of turbulent kinetic energy causes a shift in the momentum decay. In other words, the wave momentum from the breaking waves is temporarily stored as turbulent momentum and is not immediately used to generate longshore current. They solved the TKE equation and incorporated the results into a longshore current model. Using DELILAH data, their model showed only small improvements in moving the computed maximum toward the trough. In recent years, quasi-3D nearshore wave-driven current models were developed. Garcez Faria et al. (1995) investigated the effect of cross-shore current on the location of the maximum. Using SHORECIRC, Sancho et al. (1995) studied the effects of longshore nonuniformities on longshore currents. None of these models had complete success in predicting the location of maximum current. More research needs to be done.

8.0 CONCLUSIONS

In this report, we develop a variable bottom friction coefficient function based on surf zone width and depth. It is important to note that our function is not dependent on information about bottom material and roughness, which are often difficult to obtain, especially in denied areas. The physical reasons for the validity of the function have been covered in details in the discussion section. In short, the function reflects the increase of bottom friction due to the sediment sorting and compensates for the lack of vertical eddy diffusivity in 1D models. The latter becomes more important in the very shallow water due to the intensive breaking.

A comprehensive set of data from two field experiments at Duck, North Carolina, is used to develop and calibrate a variable bottom friction function that effectively increases the skill of longshore current estimates. The new bottom friction function, along with a newly selected eddy viscosity coefficient, significantly improves the magnitude and location of the maximum current, and greatly reduces the unrealistic high current near the water edge. The new model also produces lower root-mean-square errors and mean relative errors. Application of the new model to a beach at Santa Barbara, California, also shows significant improvements over the old model with the fixed bottom friction coefficient. This independent validation proves that the improved model and our approach are robust.

The improvements described by no means imply that no further work on a longshore current model is needed. Our model can be further improved in its prediction of the location of the maximum current on barred beaches. The decay of longshore current in the most shoreward quarter of the surf zone can also be

refined. However, there is a limit as to how far one can improve 1D models, which are understandably limited in the representation of all important physical processes in the surf zone. In a few years, the present 1D model may be replaced by a quasi-3D model, which covers nearshore dynamics more completely. An additional advantage of a 3D model is its possibility to predict rip currents. Until then, our improved model constitutes significant progress in longshore current prediction and will be used to upgrade SURF 3.0. It should be noted that we have demonstrated the usefulness of three data sets acquired during intensive field experiments. These data sets have been formatted in such a way that validation of future surf model improvements can be done efficiently. Any new longshore or nearshore current model needs to show consistent, accurate performance with various data sets before it can be adopted for operational use.

ACKNOWLEDGMENTS

The authors thank Prof. Edward Thornton of the Naval Postgraduate School, Prof. Robert Guza of the Scripps Institution of Oceanography, and Dr. Chuck Long of the Field Research Facility for providing the NSTS, DELILAH, and DUCK94 data sets. This work was sponsored by the Space and Naval Warfare Systems Command under program element 603207N-Coastal Wave/Surf Models Project. Dr. Ed Harrison is the program manager.

REFERENCES

Battjes, J.A., 1975: "Modeling of Turbulence in the Surf Zone," Proceedings of the Symposium on Modelling Techniques, San Francisco, ASCE, pp.1050-1061.

Battjes, J.A., 1983: "Surf Zone Turbulence," Proceedings of the 20th IAHR Congress, Moscow, International Association of Hydraulic Engineering and Research, Vol. 7, pp. 137-140.

Birkemeier, W.A., ed., 1991: informal DELILAH investigators' report, Waterways Experiment Station, U.S. Army Corps of Engineers, Vicksburg, MS.

Commander, Naval Surface Force, Pacific and Commander, Naval Surface Force, Atlantic,1987: *Joint Surf Manual*, COMNAVSURFPAC/COMNAVSURFLANTINST 3840.1B, 02 January 1987, 13 chap., 1 appendix.

Earle, M.D., 1989: *Surf Forecasting Software Scientific Reference Manual*, MEC Corporation report for ASW Oceanography Program Office, Naval Ocean Research and Development Activity (N00014-84-C-0116), 261 pp. (Available from Naval Research Laboratory [Code 7032.2], Stennis Space Center, MS 39529-5004)

Earle, M.D., 1991: *Surf Forecasting Software Improvements*, MEC Corporation report for Naval Oceanographic and Atmospheric Research Laboratory, Stennis Space Center, MS (N00014-91-C-6011), 31 pp. (Available from Naval Research Laboratory [Code 7032.2], Stennis Space Center, MS 39529-5004)

Garcez Faria, A.F., E.B. Thornton, and T.P. Stanton, 1995: "A Quasi-3D Model of Longshore Current," Coastal Dynamics '95, Gdansk, ASCE, pp. 389-400.

Garcez Faria, A.F., 1997: "Nearshore Currents over a Barred Beach," Ph.D. dissertation, Naval Postgraduate School, Monterey, CA, 167 pp.

Garcez Faria, A.F., E.B. Thornton, T.P. Stanton, and C.V. Soares, 1998: "Vertical Profiles of Longshore Currents and Related Bed Shear Stress and Bottom Roughness," *J. Geophys. Res.* **103**(C2), 3217-3232.

Howd, P.A. and W.A. Birkemeier, 1987: "Beach and Nearshore Survey Data: 1981-1984," Tech. Rep. CERC-97-9, U.S. Army Engineers Waterways Experiment Station, Vickburg, MS, 143 pp.

Hsu, Y.L., T.R. Mettlach, M.E.Earle, E.P. Kennelly, 1997: "Interim Report on Validation of the Navy Surf Model," NRL/MR/7322—97-8054, Oct.1997, 233 pp.

Jonsson, I.G., 1966: "Wave Boundary Layers and Friction Factors," *Proc. Eng. Conf., 10th*, Tokyo, Japan, Am. Soc. Civil Eng., 127-148.

Kraus, N.C. and M. Larson, 1991: "NMLONG: Numerical Model for Simulating the Longshore Current, Report 1, Model Development and Tests," Waterways Experiment Station, U.S. Army Corps of Engineers, Vicksburg, MS, June 1991, 166 pp.

Lippmann, T.C., A.H. Brookins, and E.B. Thornton, 1996: "Wave Energy Transformation on Natural Profiles," *Coast. Eng.* **27**, 1-20.

Longuet-Higgins, M.S., 1970a: "Longshore Currents Generated by Obliquely Incident Sea Waves, 1," *J. Geophys, Res.* **75**(33), 6778-6789.

Longuet-Higgins, M.S., 1970b: "Longshore Currents Generated by Obliquely Incident Sea Waves, 2," *J. Geophys, Res.* **75**(33), 6779-6801.

Lundberg, DL. and K.T. Holland, 1997: "A Semi-Empirical Longshore Current Model," NRL/MR/7442—97-8066, Oct. 1997, 39 pp.

Lundberg, DL. and K. T. Holland, 1999: "Validation of the Semi-Empirical Longshore Current Model," NRL/MR/7442—98-8092, Feb.1999, 34 pp.

May, D.A. and T.R. Mettlach, 1998: "Navy Surf Model: Comparative Performance of Alternative Initialization Parameter Sources," NRL/FR/7343—97-9670, Mar.1998, 45 pp.

Mettlach, T.R., E.P. Kennelly, and D.A. May, 1996: "Surf Forecasting Using Directional Wave Spectra with the Navy Standard Surf Model," NRL/MR/7240—96-8019, Sept. 1996, 25 pp.

Mettlach, T. R. and D.A. May, 1997: "The Accuracy of the Navy-Standard Surf Model-Derived Modified Surf Index and Its Sensitivity to Nearshore Bathymetric Errors," NRL/FR/7240—97-9665, Oct.1997, 34 pp.

Mettlach, T.R., K.T. Holland, and D.A. May, "The Accuracy of the Navy Surf Model Estimates of Surf Zone with an Examination of the Important Influences on Incipient Wave Breaking," NRL/FR/7440—99-9693, Sept. 1999.

Migues, L, D. Osiecki, M. Earle and T Mettlach, 1999: "Software Design Document for the Oceanographic and Atmospheric Master Library, SURF 3.0 Forecasting Program," Neptune Sciences, Inc., report to the Naval Oceanographic Office.

Reniers, A.J.H.M. and J.A. Battjes, 1997: "A Laboratory Study of Longshore Currents over Barred and Non-barred Beaches," *Coast. Eng.* **30**, 1-22.

Sancho, F. E., Svendsen, A.R. Van Dongeren, and U. Putrevu, 1995: "Longshore Nonuniformities of Nearshore Currents," Coastal Dynamics '95, Gdansk, ASCE, pp.425-436.

Sancho, F.E., 1999: "Unsteady Nearshore Currents on Longshore Varying Topographies," dissertation, Dept. of Civil and Environmental Eng., U. of Delaware, 319 pp.

Smith, J.M., M. Larson and N.C. Kraus, 1993: "Longshore Current on a Barred Beach: Field Measurements and Calculation," *J. Geophys. Res.* **98**(C12), 22717-22731.

Svendsen, I.A. and U. Putrevu, 1994: "Nearshore Mixing and Dispersion," Proc. Roy. Soc. A, **445**, 561-576.

Swart, D.H., 1974: "Offshore Sediment Transport and Equilibrium Beach Profile," Delft Univ. Tech. Dissertation, Delft Hydro. Lab., Pub. No. 131, 244 pp.

Thornton, E.B., 1970: "Variation of Longshore Current Across the Surf Zone, Procedings of the 12th Coastal Engineering Conference, ASCE, pp. 291-308.

Thornton, E.B and R.T. Guza, 1983: "Transformation of Wave Height Distribution," *J. Geophys. Res.* **88**(C10), 5925-5938.

Thornton, E.B and R.T. Guza, 1986: "Surf Zone Currents and Random Waves: Field Data and Models," *J. Phys. Oceanog.* **16**, 1165-1178.

Whitford, D.J. and E.B. Thornton, 1996: "Bed Shear Stress Coefficients for Longshore Currents over a Barred Profile," *Coast. Eng.* **27**, 243-262.

Appendix A
VALIDATION STATISTICS

The following definitions for various elementary skill statistics are used throughout this report. All error statistics are based on the difference $x_{model} - x_{true}$, where x_{true} is based on the measurement. For N observations the mean of the simple error ε_{mean} is given as

$$\varepsilon_{mean} = \frac{1}{N}\sum_{i=1}^{N}\left(x_{i,model} - x_{i,true}\right). \tag{A1}$$

Physical units are the same as $x_{i,model}$ and $x_{i,true}$. The percentage of the mean fractional error or 100 times the mean of the fractional error of a set of model estimates is given as

$$\varepsilon_{100} = \frac{100}{N}\sum_{i=1}^{N}\left(\frac{x_{i,model} - x_{i,true}}{x_{i,true}}\right); \mid x_{i,true} \mid > \tau, \tag{A2}$$

where the quantity τ is a threshold value chosen to prevent values of infinity. In this report, values of τ are a very small fraction of the range of values. The mean deviation from the true value is given as

$$\varepsilon_{100abs} = \frac{100}{N}\sum_{i=1}^{N}\left(\frac{\mid x_{i,model} - x_{i,true} \mid}{x_{i,true}}\right); \mid x_{i,true} \mid > \tau. \tag{A3}$$

It is important to point out that large numbers of low and near-zero values can contribute to high mean fractional errors. It is often necessary to exclude some low values to avoid distorting the results.

The maximum and minimum errors in a data set are defined as

$$\varepsilon_{\min} = \min(x_{model} - x_{true}), \tag{A4}$$

$$\varepsilon_{\max} = \max(x_{model} - x_{true}). \tag{A5}$$

The functions min( ) and max( ) denote the minimum and maximum errors in a set, respectively. Note that the function min( ) may yield a value that has an absolute value greater than the absolute value from the corresponding function max( ).

The standard deviation σ is the sample standard deviation, normalized by $N-1$ as given by

$$\sigma = \sqrt{\frac{\sum_{i=1}^{N}\left(\left[x_{i,model} - x_{i,true}\right] - \varepsilon_{mean}\right)^2}{N-1}}. \tag{A6}$$

Physical units are the same as $x_{i,model}$ and $x_{i,true}$.

The linear correlation coefficient R is defined as

$$R = \frac{\sum_{i=1}^{N} (x_i - \bar{x})_{model} (x_i - \bar{x})_{true}}{(N-1)\sigma_{model}\sigma_{true}}, \tag{A7}$$

where the sample standard deviations in the denominator are defined by Eq. (A8) and the overbar in the numerator (and in subsequent definitions) indicates a mean value. R ranges from –1 to 1. The symbol σ_j, where $j = \{\text{model, true}\}$, is not explicitly used in this paper, as in the notation σ_{model} and σ_{model} in Eq. (A6),

$$\sigma_j = \sqrt{\frac{\sum_{i=1}^{N} \left(x_{i,j} - \bar{x}_j\right)^2}{N-1}}. \tag{A8}$$

The slope m of the least-squares line through the set of data $\{x_{true}, x_{model}\}$ is given as

$$m = \frac{\sum_{i=1}^{N} \left(x_{i,true} - \bar{x}_{true}\right)\left(x_{i,model} - \bar{x}_{model}\right)}{\sum_{i=1}^{N} \left(x_{i,true} - \bar{x}_{true}\right)^2}. \tag{A9}$$

The y-intercept b is given as

$$b = \bar{x}_{model} - m\bar{x}_{true}. \tag{A10}$$

Appendix B
NOTATION

b — y intercept of linear regression curve

c — wave phase speed (m/s)

c_d — air-water drag coefficient

c_f — water-seabed friction coefficient

c_g — wave energy speed (m/s)

c_i — indexed value of c during numerical integration (m/s)

c_o — wave phase speed used for model initialization (m/s)

d — hydraulic radius of open channel flow (m)

f — wave frequency (Hz)

f_p — peak wave frequency (Hz)

g — acceleration of gravity (m/s^2)

h — still water depth (m)

h_i — indexed value of h during numerical integration (m)

k — wave number (radians/m)

k_a — apparent bed roughness length scale (m)

k_i — indexed value of k during numerical integration (1/m)

m — slope of linear regression curve

n — Manning resistance coefficient (s/m^3).

$p(H)$ — Rayleigh wave probability density function (1/m)

$p_b(H)$ — breaking wave probability density function (1/m)

r — roughness parameter (m)

u — wave orbital speed (m/s)

u_m — magnitude of the horizontal water particle velocity (m/s)

v — velocity of roller in kinetic energy equation (m/s)

x — cross-shore distance coordinate, positive seaward (m)

y — alongshore distance coordinate, positive left of x (m)

z — vertical coordinate, positive up (m)

A — area of roller (m^2)

A_i — simplified notation used in numerical solution of longshore current representing factor of horizontal mixing (kg/s)

B_i — simplified notation used in numerical solution of longshore current representing factor of bottom shear stress [kg/(m^2 s)]

C_{f0} — constant factor in the function c_f

C_i — simplified notation used in numerical solution of longshore current (N/m^2)

E_i — simplified notation used in numerical solution of longshore current

E_r — roller energy density (J/m^2)

E_w — wave energy density (J/m^2)

F_i — simplified notation used in numerical solution of longshore current representing factor contributing to longshore current (m/s)

H — root-mean-square wave height @(m)

H_b — breaker height (m)

H_{rms} — root-mean-square wave height (m)

$H_{rms,i}$ — indexed value of H_{rms} used during numerical integration (m)

H_{mo} — significant wave height (m)

L — wave length (m)

M — coefficient used in lateral mixing ν_t

N — number of grid points in numerical solution of longshore current

R — linear correlation coefficient

$S(f,\theta)$ — wave spectral energy density function [m^2/(Hz-radians)]

$S(\theta)$ — frequency-integrated wave spectral energy density (m^2/radians)

$S_{xx,r}$ — cross-shore component of cross-shore radiation stress from rollers (J/m^2)

$S_{xx,w}$ — cross-shore component of cross-shore radiation stress from waves (J/m^2)

$S_{xy}(f,\theta)$ — along-shore component of cross-shore radiation stress from waves (J/m^2)

U — wind speed (m/s)

V — longshore current (m/s)

V_i — indexed value of longshore current used in numerical integration (m/s)

V_{max} — maximum longshore current in the surf zone (m/s)

$W(H)$ — weighting function associated with Rayleigh wave distribution

X_b — surf zone width (m)

ε — wave energy dissipation (W/m^2)

ε_{100} — percent fractional error (see F)

ε_{100abs} — mean of the absolute value of the fractional error

ε_i — indexed value of ε during numerical integration (W/m^2)

ε_{max} — maximum error in model estimate compared to measurement

ε_{mean} — mean error in model estimate compared to measurement

ε_{min} — minimum error in model estimate compared to measurement

γ — coefficient of O(1) used with Thornton and Guza wave dissipation model

η — wave setup (m)

ν_t — lateral mixing eddy viscosity used in SURF 3.0 (m^2/s)

ρ — density of seawater (kg/m^3)

ρ_a — density of air (kg/m^3)

σ — angle of the wave-roller stress vector

σ — standard deviation

τ — minimum threshold value in denominator when calculating fractional error

τ_S — TKE production at wave-roller interface (J/m^2)

τ_B — longshore component of mean time-averaged bottom shear stress (N/m^2)

τ_H — wave stress in the longshore direction (N/m^2)

τ_U — wind stress in the longshore direction (N/m^2)

π — $4 \tan^{-1}(1) = 3.14159265...$

θ — wave angle (direction from; positive counterclockwise from shore normal; radians)

θ_{avg} — average wave direction

θ_i — indexed value of wave angle (direction from; positive counter-clockwise from shore normal; radians)

θ_o — wave angle used for model initialization (direction from; positive counter-clockwise from shore normal; radians)

θ_p — peak wave angle

θ_U — wind direction angle (direction from; positive counter-clockwise from shore normal; radians)

ω — angular frequency (Hz)

ξ — maximum water particle excursion amplitude of fluid motion at the bottom (m)

ζ — tide level (m)

Λ — empirical coefficient used in Kraus and Larson formula for eddy viscosity